RESEARCH ARTICLE

The INO80 chromatin remodeler sustains metabolic stability by promoting TOR signaling and regulating histone acetylation

Sean L. Beckwith, Erin K. Schwartz, Pablo E. García-Nieto, Devin A. King, Graeme J. Gowans, Ka Man Wong, Tessa L. Eckley, Alexander P. Paraschuk¤a, Egan L. Peltan¤b, Laura R. Lee, Wei Yao, Ashby J. Morrison*

Department of Biology, Stanford University, Stanford, CA, United States of America

¤a Current address: Department of Biological Sciences, Florida Atlantic University, Boca Raton, FL, United States of America
¤b Current address: Department of Chemical and Systems Biology, Stanford University School of Medicine, Stanford, CA, United States of America
* ashbym@stanford.edu

Abstract

Chromatin remodeling complexes are essential for gene expression programs that coordinate cell function with metabolic status. However, how these remodelers are integrated in metabolic stability pathways is not well known. Here, we report an expansive genetic screen with chromatin remodelers and metabolic regulators in *Saccharomyces cerevisiae*. We found that, unlike the SWR1 remodeler, the INO80 chromatin remodeling complex is composed of multiple distinct functional subunit modules. We identified a strikingly divergent genetic signature for the Ies6 subunit module that links the INO80 complex to metabolic homeostasis. In particular, mitochondrial maintenance is disrupted in *ies6* mutants. INO80 is also needed to communicate TORC1-mediated signaling to chromatin, as *ino80* mutants exhibit defective transcriptional profiles and altered histone acetylation of TORC1-responsive genes. Furthermore, comparative analysis reveals subunits of INO80 and mTORC1 have high co-occurrence of alterations in human cancers. Collectively, these results demonstrate that the INO80 complex is a central component of metabolic homeostasis that influences histone acetylation and may contribute to disease when disrupted.

Author summary

Cells coordinate their metabolism with the nutrient environment in order to adapt and thrive. One of the key ways that cells regulate their metabolism is through changes in metabolic gene expression. The transcription of genes is often regulated by manipulating chromatin, which is the packaging material of eukaryotic genomes. Chromatin can be dynamically modified by post-translational modifications, such as histone acetylation, and by ATP-dependent chromatin remodeling complexes. We performed an extensive genetic screen in the budding yeast *Saccharomyces cerevisiae* in order to identify chromatin regulators of cellular metabolism. We found that the INO80 chromatin remodeling

complex is required to maintain proper levels of histone acetylation at metabolic genes and is important for the TOR metabolic signaling pathway. Additionally, cancer patients frequently have alterations in both INO80 genes and TOR genes, suggesting that disruption of both these components may facilitate the metabolic aberrations that are a hallmark of many cancer cells.

Introduction

Chromatin is a complex structure that is dynamically reorganized to facilitate DNA-templated processes such as transcription, chromosome segregation, DNA replication and DNA repair. Enzymes that restructure the chromatin environment are critical components of epigenetic maintenance and can contribute to disease when disrupted. Included among chromatin modifiers are enzymes that post-translationally modify histones and ATP-dependent chromatin remodelers that alter the position and composition of nucleosomes [1]. Chromatin remodelers are evolutionarily conserved and regulate diverse processes required for normal cell function, organismal development and are mutated in a large fraction of cancers [2,3].

Many remodelers are large multi-subunit complexes that can utilize the function of different subunits in a tissue-specific manner, allowing for cell-type specific regulation [4]. In particular, different subunits of the evolutionarily conserved INO80 chromatin remodeling complex have demonstrated roles in diverse processes, such as transcription [5–7], replication [8–10], DNA damage responses [11–14], telomere regulation [15], mitotic stability [16,17], and metabolic homeostasis [18]. These studies exemplify the functional diversity of the INO80 complex in different pathways [19–21], and suggest the partitioning of diverse functions among the subunits of the INO80 complex.

Individual subunits of the INO80 complex assemble within distinct structural modules along the ATPase subunit [22,23]. The Actin-related protein 8 (Arp8) module consists of Arp8, Arp4, Actin, Taf14 and Ies4. Arp4 and Arp8 are important for nucleosome recognition, ATP hydrolysis, and nucleosome sliding *in vitro* [22,24–28]. The N-terminal domain of the Ino80 ATPase assembles the Nhp10 module consisting of Nhp10, Ies1, Ies3, and Ies5, subunits that are less conserved among different species [22,29]. The Arp5 module is essential for chromatin remodeling activity and includes Arp5 and Ies6 subunits that are needed for ATP hydrolysis, nucleosome sliding, and histone exchange [22,23,28,30].

One recent example of specific subunit contribution to the function of the INO80 complex is the role of the Arp5 and Ies6 subunits in the regulation of metabolic gene expression [18]. Specifically, Arp5 and Ies6 form an abundant subcomplex that can assemble into the INO80 complex, stimulating *in vitro* activity and activating carbon metabolism gene expression *in vivo*. Indeed, these results support an emerging model where chromatin modifying enzymes are responsive to the metabolic state of the cell and alter the chromatin landscape, thereby linking metabolic status to transcriptional responses [31]. Indeed, many chromatin-modifying enzymes use key metabolites as co-factors or substrates that can fluctuate in different metabolic conditions, including acetyl-CoA, nicotinamide adenine dinucleotide (NAD^+), and ATP. For example, histone acetyltransferases (HATs) use nuclear acetyl-CoA in high glucose conditions to acetylate histones, creating a permissive state for transcription [32]. Additionally, in low energy states, high NAD^+ levels activate the SIRT1 histone deacetylase (HDAC) to deacetylate H3K9 at the rDNA loci, suppressing the highly energy-consuming process of ribosome biogenesis [33]. Lastly, chromatin remodeling enzymes use ATP to hydrolyze histone-DNA contacts as they reposition or restructure nucleosomes [34].

In order to identify the *in vivo* mechanisms of INO80's metabolic regulation, we created a genetic interaction map using the epistatic mini-array profile (EMAP) approach in *S. cerevisiae*. Genetic interactions can reveal how sets of proteins coordinate higher level biological functions and identify crosstalk between pathways and processes [35]. EMAPs have previously been used to decipher gene networks involved in the secretory system [36], chromatin modification [37], and DNA damage responses [38,39].

We identified genetic interactions between many chromatin and metabolic regulators, in both nutrient rich media and metabolic stress conditions to reveal nutrient-specific interactions. Our work reveals that subunits of the INO80 complex are functionally diverse and define distinct genetic modules. Both the NHP10 and ARP5 genetic modules connect the INO80 complex to histone (de)acetylation. Interestingly, we find that the IES6 genetic module is relatively disconnected from the rest of the INO80 complex and genetically interacts with components of the Target of Rapamycin (TOR) pathway that are critical to the maintenance of metabolic homeostasis. These results place the INO80 complex as an important regulator of histone modification that is downstream of TOR signaling.

Results

An EMAP of chromatin and metabolic regulators

Given the interplay between metabolism and epigenetics, we set out to comprehensively identify shared pathways in which chromatin and metabolic regulators function in *S. cerevisiae*. To do this, we conducted an EMAP of unstressed and metabolically challenged cells grown on rich media (untreated), rapamycin or ethanol, which generated approximately a quarter million interactions (Fig 1A and S1 Table). Rapamycin inhibits the TORC1 complex, a master regulator of cellular growth [40]. Ethanol is a non-fermentable carbon source that requires cells to utilize oxidative phosphorylation, whereas yeast preferentially ferment glucose [41]. We included a test library of 1536 alleles covering most major cellular processes, and significantly enriched for chromatin and metabolic regulators [42]. We used 54 query strains that cover several chromatin remodeling complexes, histone modifiers and metabolic signaling pathways (Fig 1B).

Our analyses also included deletions of all INO80's unique subunits and domain mutants of *INO80*, *ARP5* and *IES6* (see *Materials and Methods*) because complete deletion resulted in inconsistent colony growth in the EMAP process, thus confounding our ability to confidently determine genetic interactions. The resulting mutants disrupted the Arp8, Arp5 and Nhp10 structural modules of the INO80 complex (S1 Fig).

Genetic interactions (S-scores) were calculated from the fitness of double mutants (Fig 1C and S2 Fig). Positive (suppression/alleviating) S-scores often reveal epistatic genetic relationships and indicate that the fitness of the double mutant was better than expected. Negative (synthetic sick/aggravating) S-scores usually identify compensatory pathways and indicate worse fitness than expected [43]. Differential interaction networks for rapamycin and ethanol were assessed by comparing interactions in treated and untreated growth conditions (Fig 1D and S3 Fig and S4 Fig), as previously described [38].

Over 5000 significant interactions were identified in both the untreated and rapamycin differential networks (Fig 1E and S2 Table). In the presence of rapamycin, several TOR pathway genes, such as the TORC1 effector kinase *SCH9* and TORC1 subunit *LST8* have increased number of significant interactions, indicating that the differential network is broad and effective at identifying TOR dependent genetic interactions (Fig 1F). Several subunits of the INO80 chromatin remodeling complex (*IES2*, *IES4*, *IES6*) also have increased number of interactions in the rapamycin differential network, supporting a metabolic role for INO80. In contrast, the
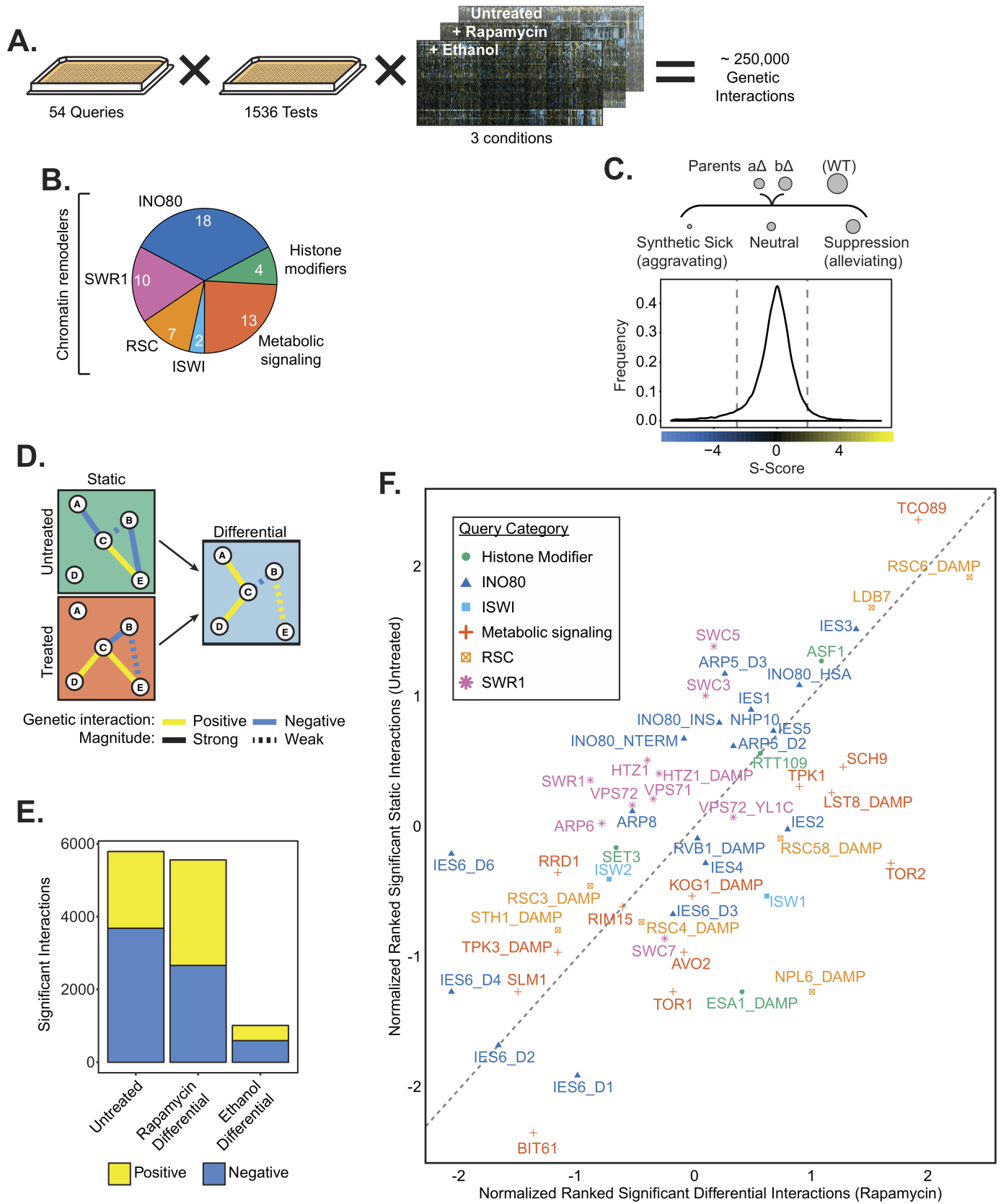
Fig 1. An epistasis map of chromatin and metabolic regulators. (A) Overview of EMAP including 54 query strains and a library of 1536 test strains, assayed in three growth conditions. **(B)** Composition of the query library by number of query strains; INO80, SWR1, RSC and ISWI are chromatin remodeling complexes. Histone modifiers include histone acetyl-transferases and histone deacetylases. Metabolic signaling genes include components of the TOR and PKA signaling networks. Numbers indicate the number of query strains in each category. **(C)** *Top*, Genetic interaction scores (S-score) are computed by comparing the observed fitness, inferred from colony size, of double mutants with the expected fitness, which is based on fitness of parental strains. A wild-type (WT) strain is shown for comparison. *Bottom*, the distribution of S-scores is shown for the untreated condition. Dashed lines indicate significance cutoffs of -2.5 and 2 for aggravating and alleviating interactions, respectively. **(D)** Hypothetical genetic interaction network indicating how the differential network is constructed by "subtracting" the untreated condition from treated condition. **(E)** The number of significant positive and negative interactions for each growth condition. **(F)** Plot of rankit normalized significant interactions by query gene in the untreated condition and the rapamycin differential condition. Color and shape indicate query gene category. Dashed line indicates y = x reference line. Significant interaction tallies are included in S2 Table.

https://doi.org/10.1371/journal.pgen.1007216.g001

ethanol differential network yielded fewer genetic interactions and only a few query strains have increased significant interactions, suggesting a less dramatic reorganization of the genetic interaction landscape upon ethanol treatment than in response to rapamycin (Fig 1E and S5 Fig). Interestingly, four of the top five query strains with the most significant interactions in the ethanol differential condition were subunits of the INO80 complex (S2 Table). As observed before, *arp5Δ* and *ies6Δ* mutants have higher growth rates than expected on ethanol, presumably because these mutants have increased respiratory capacity [18]. These genetic results further highlight a critical function for INO80, and the Arp5-Ies6 module, as an interaction hub for cellular response to ethanol.

Distinct genetic organization of the INO80 and SWR1 complexes

We first used our EMAP data to comprehensively map the functional modules within the INO80 complex by correlating the interaction profile of each query subunit across the test library in untreated growth conditions (Fig 2A). Using this method, we found that INO80 subunits were organized into 4 genetic modules, which were also independently identified in principal component analysis (PCA) when pairwise correlations were k-means clustered (Fig 2B). Notably, the Nhp10 structural module clustered genetically and included Nhp10, Ies1, Ies3, Ies5, and the Ino80 N-terminus on which the Nhp10 module assembles. Thus, the distinct *in vivo* function of the NHP10 genetic module is organized among the subunits that are physically associated. [Note, for clarity, genetic modules are denoted with all uppercase letters (e.g. NHP10 module) and structural modules are denoted with an uppercase first letter only (e.g. Nhp10 module)].

However, other subunits of the INO80 complex assemble in genetic modules that are distinct from their structural modules. For example, Ies4 is structurally in the Arp8 module but was slightly more genetically similar to the NHP10 genetic module (Fig 2A and 2B). In addition, although Arp8 and Arp5 form separate structural modules, their genetic profiles are similar and constitute the ARP5 genetic module, which also includes *IES2*. Ies2 is needed for the Arp5 structural module to assemble with the INO80 complex [30], thus its *in vivo* function is tightly connected to Arp5 and is reflected in our genetic analysis.

The genetic signatures of the *INO80* helicase-SANT-associated (HSA) and insertion domain mutants were closely associated with each other and clustered closest to many subunits that assemble within those domains (Fig 2A and 2B). Namely, the HSA domain is required for association of Arp8 [44] (S1A and S1B Fig); and the insertion domain that splits *INO80*'s ATPase is required for the association of the Arp5 structural module [30]. Most strikingly, all the domain mutants of *IES6* had genetic profiles that were dissimilar to the rest of the INO80 complex (Fig 2B). In fact, *IES6* mutant signatures anti-correlated with those in the ARP5 genetic module (Fig 2A). As previously mentioned, Arp5 and Ies6 are physically associated and form an independent subcomplex [18,22,30], thus their divergent genetic profiles were extremely surprising. This genetic data suggests that, although Arp5 and Ies6 are physically
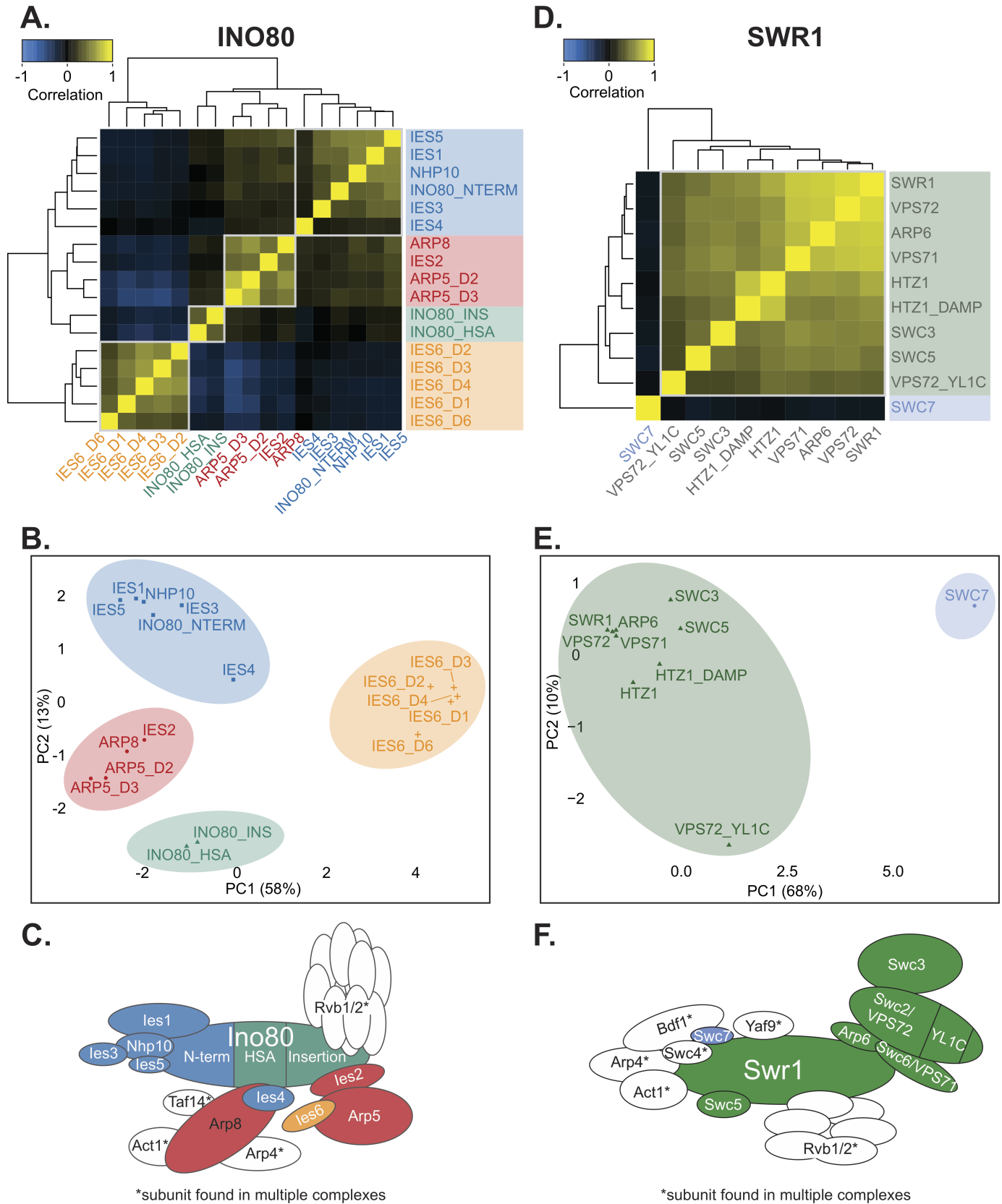
Fig 2. The INO80 complex is composed of distinct genetic modules. (A) Heatmap illustrating pairwise Pearson correlations between INO80 complex subunit query strains across the test library in the untreated static condition. Boxes outline genetic modules identified by hierarchical clustering and k-means analysis. Subunits that are not unique to the INO80 complex were omitted from the analysis. Mutants are complete deletion or domain deletions where indicated: *INO80* N-terminal (NTERM), insertion (INS), and HSA deletions; *ARP5* domain 2 and 3 (D2 and D3) deletions; and *IES6* domain 1, 2, 3, 4, and 6 (D1, D2, D3, D4, D6) deletions. **(B)** Principal component analysis (PCA) of Pearson correlations of INO80 complex subunit query strains as in (A). Colors indicate clustered genetic modules identified by k-means clustering (k = 4). **(C)** Schematic illustrating the INO80 complex organized by known physical interactions [22,23] with colors representing genetic modules of INO80 subunits identified in the untreated EMAP. **(D)** Heatmap of SWR1 complex subunit query strain Pearson correlations, as in (A). Mutants are complete deletion or domain deletions where indicated, *d*ecreased *a*bundance by *m*RNA *p*erturbation (DAmP) alleles are as described in [36]. A Vps72 (Swc2) YL1-C domain mutant that is conserved in Ies6 was also included. **(E)** PCA of SWR1 strains as in (B), with k = 2. **(F)** Schematic illustrating the SWR1 complex as in (C) based on structural studies [46].

coupled, they have some distinct and separable cellular functions. Fig 2C illustrates the INO80 complex genetic modules by color and are arranged according to previously identified structural modules [22]. INO80's genetic architecture was not substantially changed in the rapamycin or ethanol EMAP (S6A–S6D Fig).

In contrast to the INO80 complex, the SWR1 complex, another member of the INO80 chromatin remodeling subfamily [45], formed a strikingly cohesive genetic module (Fig 2D, 2E and 2F). As before, analysis of non-unique subunits was not performed, such as several subunits that assemble in the N-terminal module of SWR1 [46] and are also found in the NuA4 acetyltransferase complex. Notably, our genetic analysis highlighted Swc7 as an outlier, the genetic profile of which did not correlate with other SWR1 subunits and formed a distinct module in PCA analysis and k-means clustering (Fig 2D and 2E). Fig 2F summarizes the genetic modules for SWR1, which are arranged according to previously identified structural modules [46]. These genetic modules were largely preserved in the rapamycin and ethanol EMAP (S6E–S6H Fig).

We next broadened our analysis to compare the SWR1 and INO80 complexes together to identify subunits that may facilitate cooperative or distinct function. Interestingly, the *SWC7* genetic profile was most similar to that of the *IES6* domain mutants (S7 Fig), suggesting that these subunits have common function that is distinct from both the SWR1 and INO80 complexes. In addition, the genetic profile of the *INO80* HSA and insertion domain mutants correlated with other SWR1 subunits and clustered with SWR1 subunits in PCA analysis. This suggests that the Ino80 ATPase and the SWR1 complex are involved in similar activities *in vivo*. Indeed, INO80 and SWR1 have many overlapping reported functions, including transcriptional regulation and genome maintenance [20,47]. Additionally, high-resolution positional data shows similar binding profiles at +1 nucleosomes for both INO80 and SWR1 complex subunits [48], thus they may cooperatively regulate many genic loci.

Collectively, the EMAP results of the INO80 and SWR1 complex show very different genetic organization despite being of the same chromatin remodeling subfamily. Specifically, unique SWR1 C-terminus subunits are focused within similar *in vivo* functions, while the activities of the INO80 subunits are relatively more diverse and organized in distinct subunit modules. In addition, these analyses reveal that both Ies6 and Swc7 may not cooperatively function with their respective complexes, which might reflect independent activities for these subunits and/or regulatory roles that are not tested in the experimental conditions of this EMAP.

Metabolic functions of the INO80 complex

In order to identify the cellular pathways in which the INO80 complex functions, we examined the function of genetically interacting test genes. Test genes with significant interactions to each genetic module were identified using DAVID functional annotation clustering analysis [49,50] (Fig 3A and S3 Table), and individual biological process gene ontology enrichments
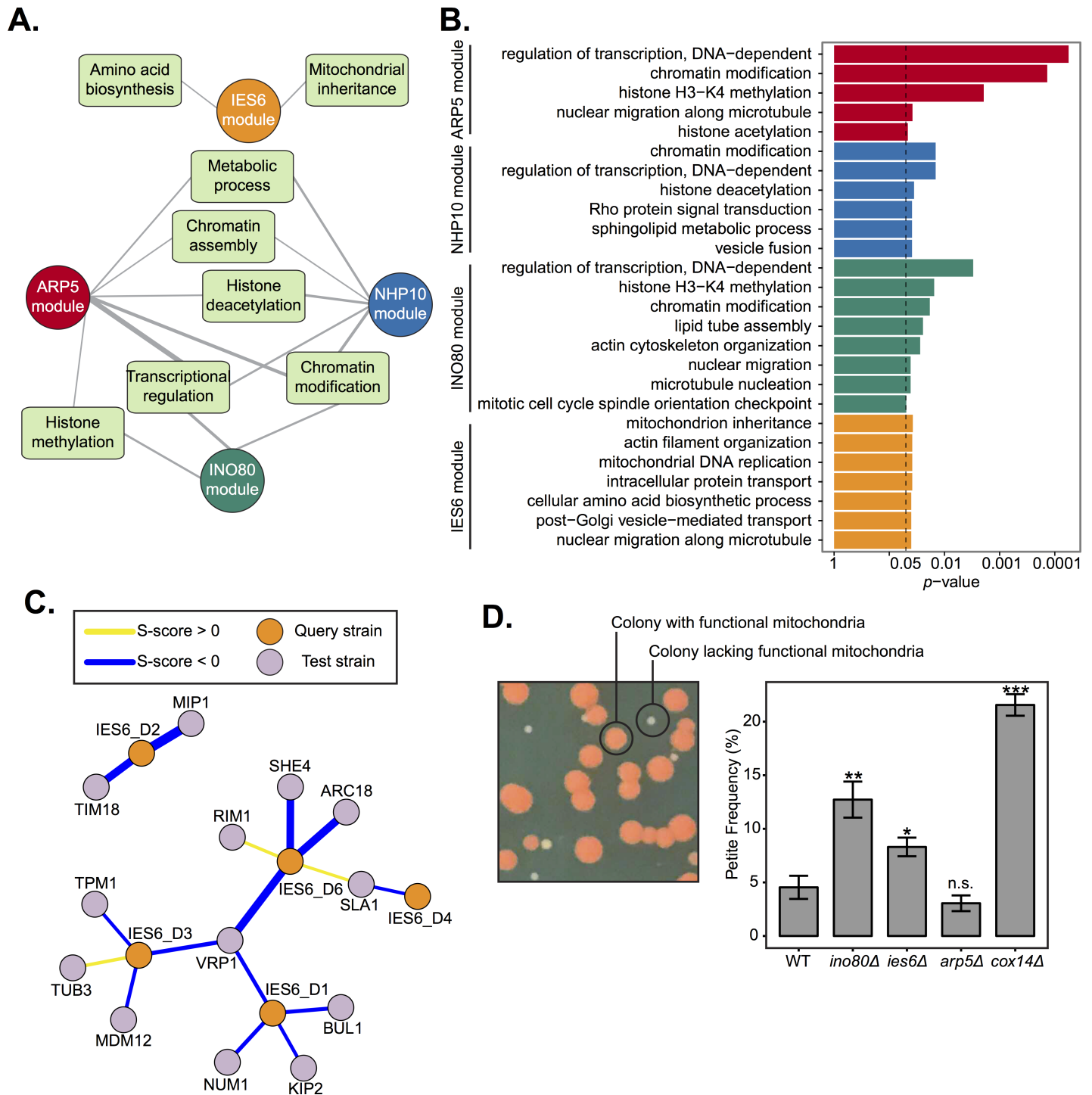
Fig 3. The IES6 genetic module is involved in mitochondrial maintenance. (A) Network diagram illustrating DAVID functional annotation clusters of significantly interacting test genes with each INO80 subunit query gene module identified in Fig 2. Line width indicates enrichment score, with a cutoff of ≥1.3 (-log₁₀ *p*-value). Genes within each annotation are listed in S3 Table. **(B)** FDR adjusted *p*-values of gene ontology (GO) enrichments (hypergeometric test, *p* < .05) of significantly interacting test genes with each INO80 subunit query gene module. The complete list of significant GO terms is found in S4 Table. **(C)** Genetic interaction network between the IES6 genetic module and significantly interacting test genes found in the DAVID mitochondrial inheritance cluster. Line width indicates strength of S-score. **(D)** *Left*, representative image of yeast colonies overlaid with tetrazolium. Colonies founded by respiratory competent cells are large and red, "petite" colonies founded from respiratory deficient cells are smaller and white. *Right*, quantification of petite frequency in the indicated strains; deletion of *COX14* is known to increase petite frequency [52]. Error bars represent standard error of the mean. Significance was determined using a Wilcoxon rank sum test from at least 8 independent measurements compared to wild-type.

are shown (Fig 3B and S4 Table). Known functions of INO80 were captured in the EMAP, for example, chromatin modification, transcriptional regulation, and chromatin assembly are significantly enriched. Histone (de)acetylases and histone methylases were also identified as significant interactors, possibly due to cooperative functions as transcriptional regulators or direct effects by histone modifications on INO80's activity. Mitotic functions, such as microtubule nucleation and mitotic spindle orientation were also identified in the INO80 genetic module, likely reflecting INO80's role in chromosome segregation [16,51].

Notably, the IES6 module did not overlap with the functional annotation clusters of the other modules and were significantly enriched in metabolic annotations, such as amino acid biosynthesis (Fig 3A), supporting previous findings of Ies6 in metabolic homeostasis [18]. The only other significantly enriched annotation observed for the IES6 genetic module was mitochondrial inheritance. Corresponding test genes that interact with *IES6* domain mutants include several involved in cytoskeleton organization, such as *VRP1*, *ARC18* and *SLA1*, and mitochondrial membrane function and DNA replication, including *TIM18* and *MIP1* (Fig 3C).

To determine if Ies6 is directly involved in mitochondrial inheritance we utilized the previously established petite assay that examines the frequency of mitochondrial dysfunction [52]. Deletion of the electron transport chain gene *COX14* served as a positive control and exhibited high petite frequency, as previously observed [52] (Fig 3D). Genetic deletions of *INO80* and *IES6* exhibited high petite frequencies, while deletion of *ARP5* did not. As previously mentioned, the difference between the *ies6Δ* and *arp5Δ* mutants is surprising given that they physically interact each other [18]. This assay further supports the notion that Ies6 and Arp5 have separable *in vivo* functions. Furthermore, unlike *ies6* mutants, mitochondrial function is not reflected in the significant genetic interactions of the *ino80* HSA and insertion domain mutants. Thus, it is likely that Ino80 function is quite varied and reflected by an extensive distribution of genetic interactions in different pathways, while Ies6 function is more specialized and enriched in mitochondrial maintenance. Collectively, these results demonstrate that the Ies6 subunit is needed for specific metabolic functions of the INO80 complex, including mitochondrial maintenance.

INO80 is a regulator of histone acetylation

To further explore how INO80 functions among the other chromatin regulators in the EMAP, we examined the genetic interaction correlations between each query strain across the entire test library (Fig 4A). Interestingly, INO80 subunits were positively correlated with Rtt109 and Asf1, components of the H3K56 acetylase pathway that are important for genome stability [37] (Fig 4A blue panel). Notably, H3K56ac has been reported to impact the histone variant exchange of Htz1 by INO80 and SWR1 *in vitro*, and high levels of H3K56ac leads to a decreased level of promoter-proximal Htz1 *in vivo* [53]. In order to investigate if these genetic similarities stem from shared transcriptional functions, we examined published microarray gene expression profiles [54] and found substantial correlations between INO80 subunits, Rtt109, and Asf1 (Fig 4B).

To explore whether Rtt109/Asf1 is a unique genetic interaction with INO80 or if INO80 is more broadly involved in histone modification status we next examined the genome-wide co-occupancy of the INO80 complex and all uniformly processed histone modification ChIP-seq datasets currently available (see *Materials and Methods*; S5 Table). We observed that Arp5 has the highest correlation with histone acetyl marks and anti-correlates with most histone methyl marks (Fig 5A). Corroborating the genetic interaction correlations between Rtt109, Asf1, and INO80 subunits, H3K56ac significantly correlates with Arp5 genome-wide (r = 0.53).

We then investigated the genetic interactions between INO80 query subunits and histone acetyltransferase and deacetylase test genes to further understand the relationship between
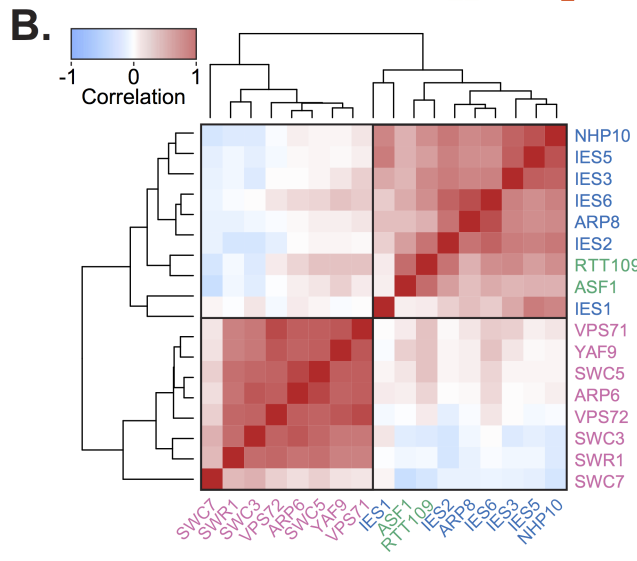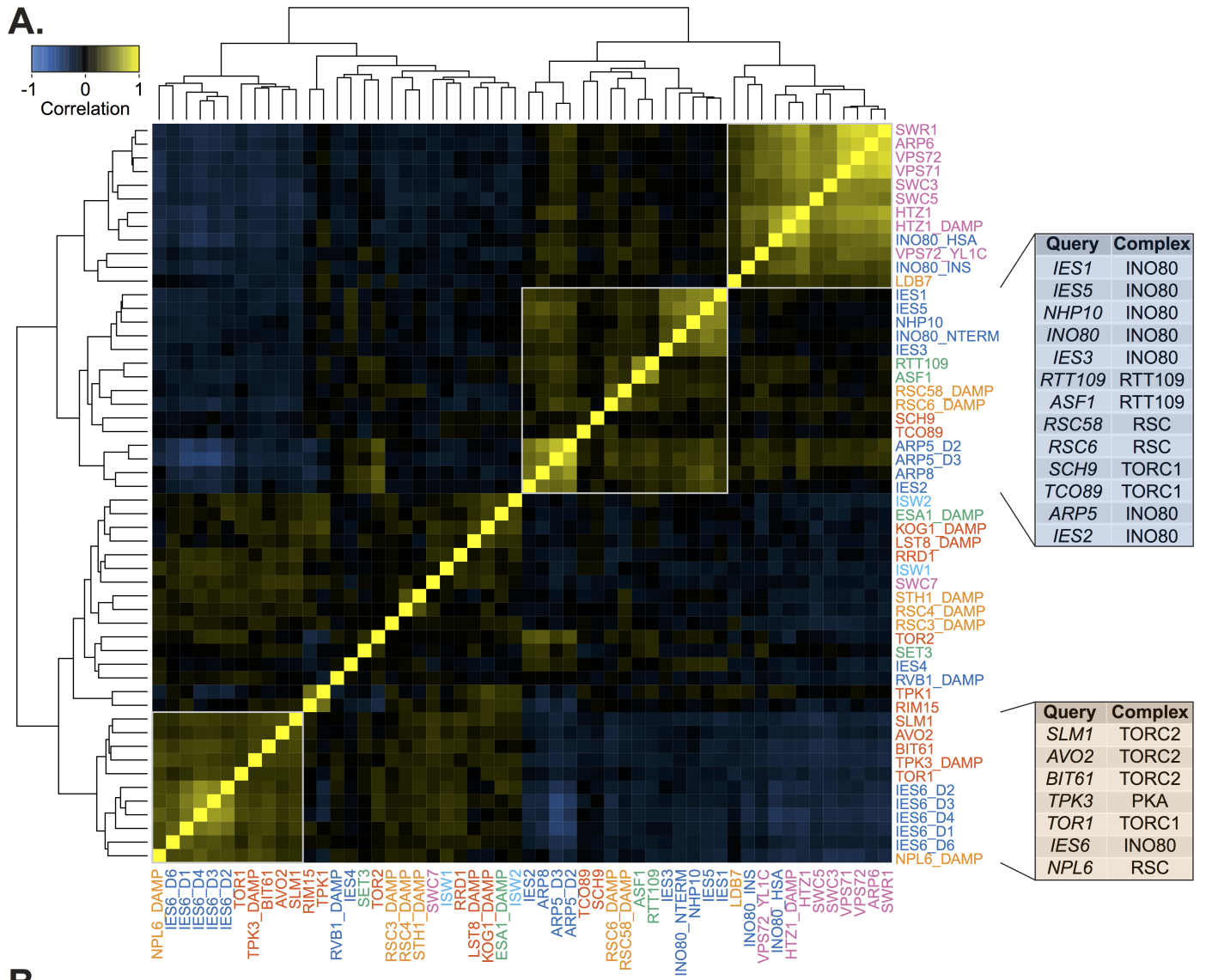
Fig 4. Genetic profiles of Rtt109 and metabolic regulators correlate with INO80. (A) Heatmap of Pearson correlation of all query strains in the untreated static condition. Label colors correspond to the query category annotated in Fig 1B. INO80 and SWR1 subunit mutants are described in Fig 2A and 2D. Boxes outline clusters identified by hierarchical clustering. *Right*, tables show the complex each query gene is found in for the INO80 and IES6 expanded genetic modules. **(B)** Heatmap of Pearson correlations of gene expression profiles from published microarray data [54] between deletion of subunits of the INO80 complex, SWR1 complex, *RTT109* and *ASF1*. All correlations between *RTT109*, *ASF1*, and INO80 subunits are significant, $p < 0.001$. Boxes indicate hierarchical clusters.

INO80 and histone (de)acetylation. We found that INO80 has the highest density of significant interactions with the Rpd3L and HDA1 histone deacetylases in untreated, nutrient rich, conditions (Fig 5B and 5C). Rapamycin treatment did not significantly alter the genetic interactions between INO80 and HDA1 (Fig 5C bottom panel). However, the interaction network density with Rpd3L was significantly increased in the differential EMAP. This result is consistent with previous findings that Rpd3L, not HDA1, regulates histone deacetylation at TORC1-responsive genes [55,56]. Additionally, the network density between INO80 and both the Hst3 sirtuin histone deacetylase and SAGA histone acetyltransferase significantly increases in the presence of rapamycin (Fig 5C bottom panel for Hst3 and S6 Table for SAGA). Both SAGA and Hst3 regulate the acetylation status of shared histone targets, the deacetylation of which is suppressed by TORC1 [57]. Thus, the INO80 complex likely functions with different (de)acetylases depending on the metabolic environment.

To further investigate INO80's maintenance of histone acetylation, we directly tested the effect of Ino80 loss on H3K18 acetylation (H3K18ac). We chose H3K18 because it is TORC1-responsive and deacetylated by Rpd3L and Hst3 [57]. Additionally, H3K18ac and Arp5 have similar average distributions around +1 nucleosomes genome-wide (S8A Fig), thus are able to regulate the same genes. We also found high H3K18ac levels at the +1 nucleosome of genes that significantly regulate the yeast metabolome [58] (Fig 5D). Accordingly, genes with high H3K18ac at the +1 nucleosome are also highly enriched for metabolome regulators (S8B Fig). H3K18ac likely serves as a proxy for several histone acetylations at metabolic loci, as H3K18ac occupancy significantly correlates (median r = 0.90) with several other acetyl marks at the +1 nucleosome genome-wide (S9 Fig). We found that following deletion of *INO80*, H3K18ac was significantly reduced at several INO80-regulated genes (Fig 5E). Collectively, these results indicate that the INO80 complex cooperates with histone (de)acetylases to enact TORC1-mediated gene expression responses.

INO80 is an effector of TOR signaling

We found strong evidence to support the role of INO80 as a TOR effector, as subunits of both TOR complex 1 and 2 (TORC1 and TORC2, respectively) and Sch9 downstream signaling kinase have positively correlated genetic interaction profiles with INO80 subunits (Fig 4A). Strikingly, 5 of the 6 genes that correlate with the IES6 genetic module are subunits of the TORC1/2 and PKA signaling pathways and form an expanded IES6 metabolic module. This IES6 metabolic module was significantly enriched in test genes involved in many metabolic processes, such as amino acid biosynthesis, mitochondrial signaling, and intracellular transport (S10A Fig and S7 Table). Treatment with rapamycin markedly reduced the strength of the genetic interaction correlations for the expanded IES6 metabolic module, confirming that the genetic interactions between query and test genes are specific to nutrient-rich conditions and are significantly reduced when TORC1-signaling is inhibited (S10B Fig). INO80 and genes in the TORC1 pathway have a highly connected genetic interaction network, both in rich media (Fig 6, $p = 1.1e-3$) and even more significantly in the rapamycin differential condition (S11 Fig, $p = 1.6e-4$), further supporting the interplay between INO80 and the TORC1 pathway.
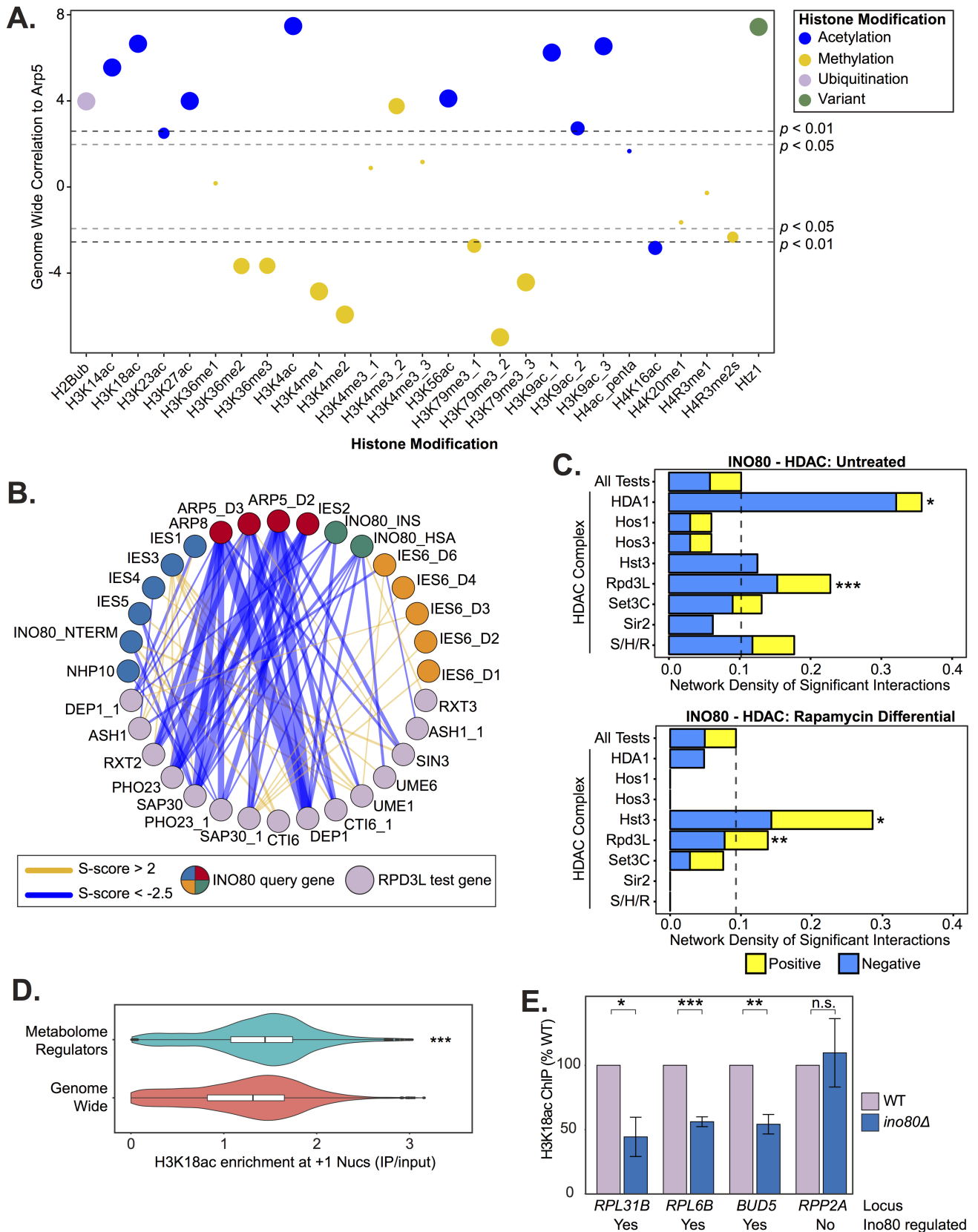
Fig 5. INO80 is a regulator of histone acetylation. (A) Genome-wide correlation of occupancy between Arp5 and histone modifications, listed on X-axis, using uniformly processed ChIP-seq data (see *Materials and Methods*). Colors illustrate modification type and size corresponds to binned *p*-value. **(B)** Genetic interaction network between INO80 subunit query strains and significantly interacting Rpd3L subunit test strains in the untreated static condition. Line width indicates strength of S-score, INO80 queries are colored according to modules identified in Fig 2. **(C)** Bar chart of network density by positive or negative significant interactions of test strains in the histone deacetylates complexes (HDACs) in yeast and INO80 subunit query strains in untreated or rapamycin differential conditions. Dashed line indicates the network density of all test strains (All Tests) and serves as a background benchmark. S/H/R is Sum1/Hst1/Rfm1. Significance was determined by Monte Carlo randomization test. **(D)** Violin and box plots of +1 nucleosome H3K18ac levels show significant regulators of the metabolome [58] (adjusted *p*-value < 0.01) have high H3K18ac levels compared to genome wide (*p*-value < 4.4e-16 by Wilcoxon rank sum test; *p* = 1.0e-5 by Monte Carlo randomization test). **(E)** ChIP-qPCR of H3K18ac in wild-type (WT) and *ino80Δ* deletion strains at loci chosen by H3K18ac levels from published data [69] and regulation of expression by Ino80 [18]. Significance was determined by Students *t*-test from at least 3 biological replicates, error bars represent standard error of the mean. Below each loci label is noted whether the gene's expression is Ino80 regulated.

https://doi.org/10.1371/journal.pgen.1007216.g005

These results prompted us to further investigate how INO80 functions with TORC1 signaling. Interestingly, RNA-sequencing comparisons between rapamycin-treated cells and *ino80Δ* or *arp5Δ* mutant strains found similarities in gene expression profiles (r = 0.34, 0.31,
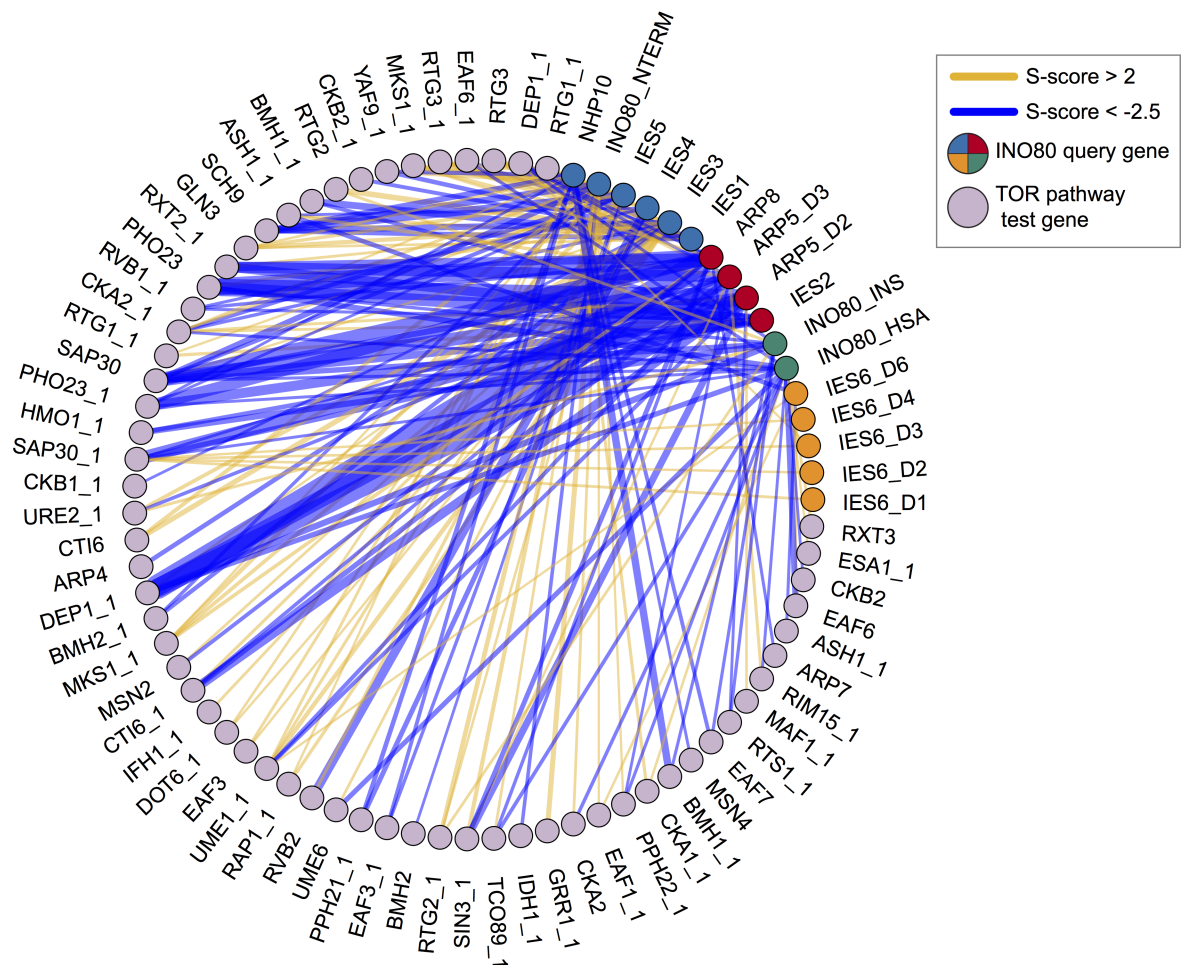
Fig 6. INO80 and the TOR pathway have a highly connected genetic interaction network. Genetic interaction network between INO80 subunit query strains and significantly interacting TOR pathway test strains in the untreated static condition. Line width indicates strength of S-score, INO80 queries are colored according to modules identified in Fig 2. Network density is significantly high, *p*-value = 1.1e-3 by Monte Carlo randomization test.

https://doi.org/10.1371/journal.pgen.1007216.g006

respectively) (Fig 7A). A similar correlation (r = 0.34) was found comparing microarray expression data between *ies2Δ* [54] and rapamycin-treated cells [59]. In fact, of the over 150 chromatin mutants analyzed [54], the expression profile of *ies2Δ* has the third highest
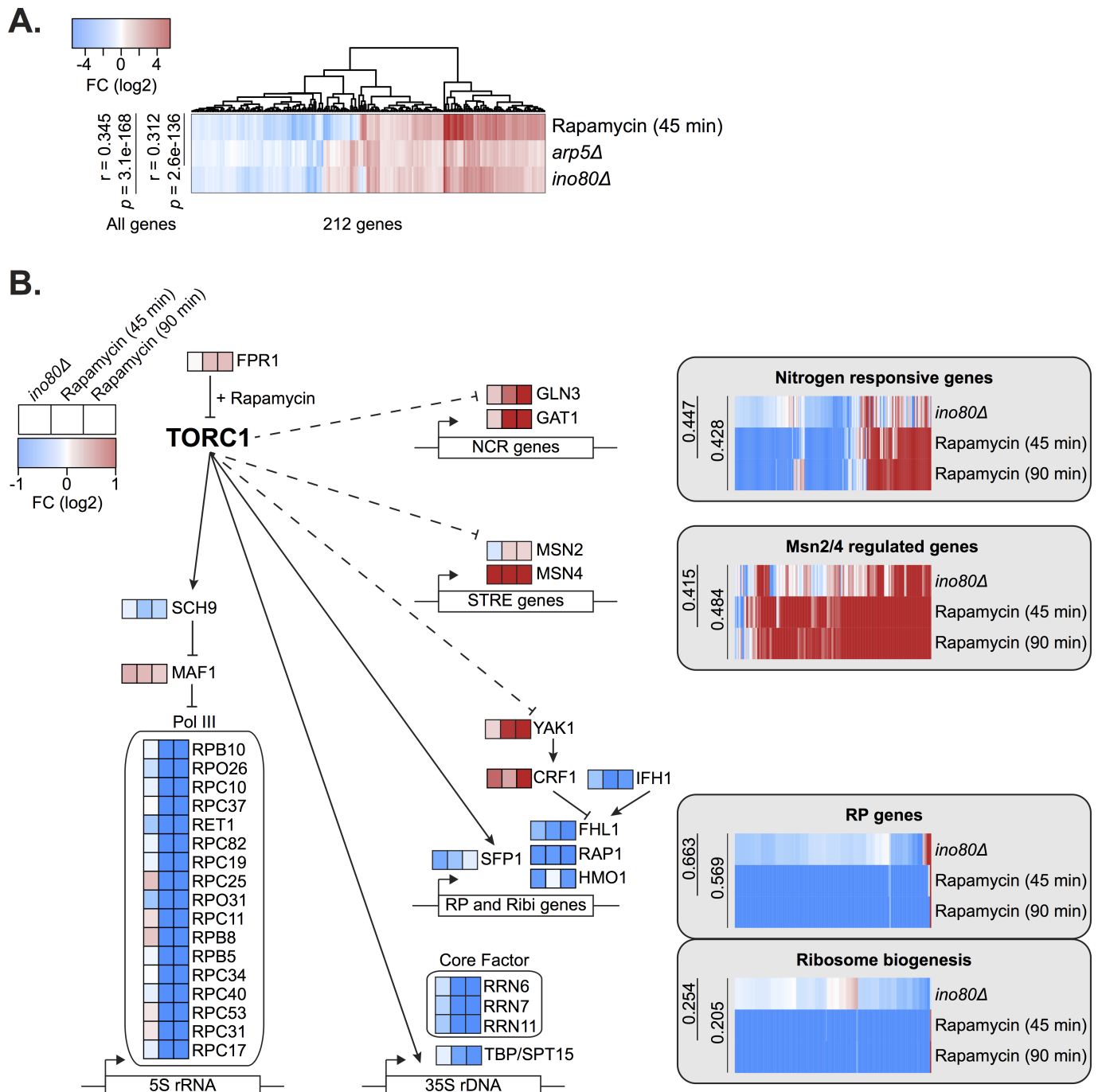
Fig 7. INO80 regulates the expression of key TOR signaling effectors. (A) Log-transformed Z-scores of expression fold-change (FC) between untreated and treated (30nM rapamycin for 45 minutes) wild-type cells or indicated deletion strains. Genes with at least a 1.5 fold-change are plotted. Pearson correlations and *p*-values are shown for all genes (>6000) regardless of fold-change difference. (B) Diagram of key genes involved in the TORC1 regulation of nitrogen source quality responsive genes [77], Msn2/4 regulated stress response genes [78], ribosomal protein (RP) genes, and ribosome biogenesis genes [79]. Log-transformed expression fold-change is shown comparing untreated wild-type cells and rapamycin treated (45 and 90 minutes) or deletion strains as indicated. Gene lists are found in S8 Table.
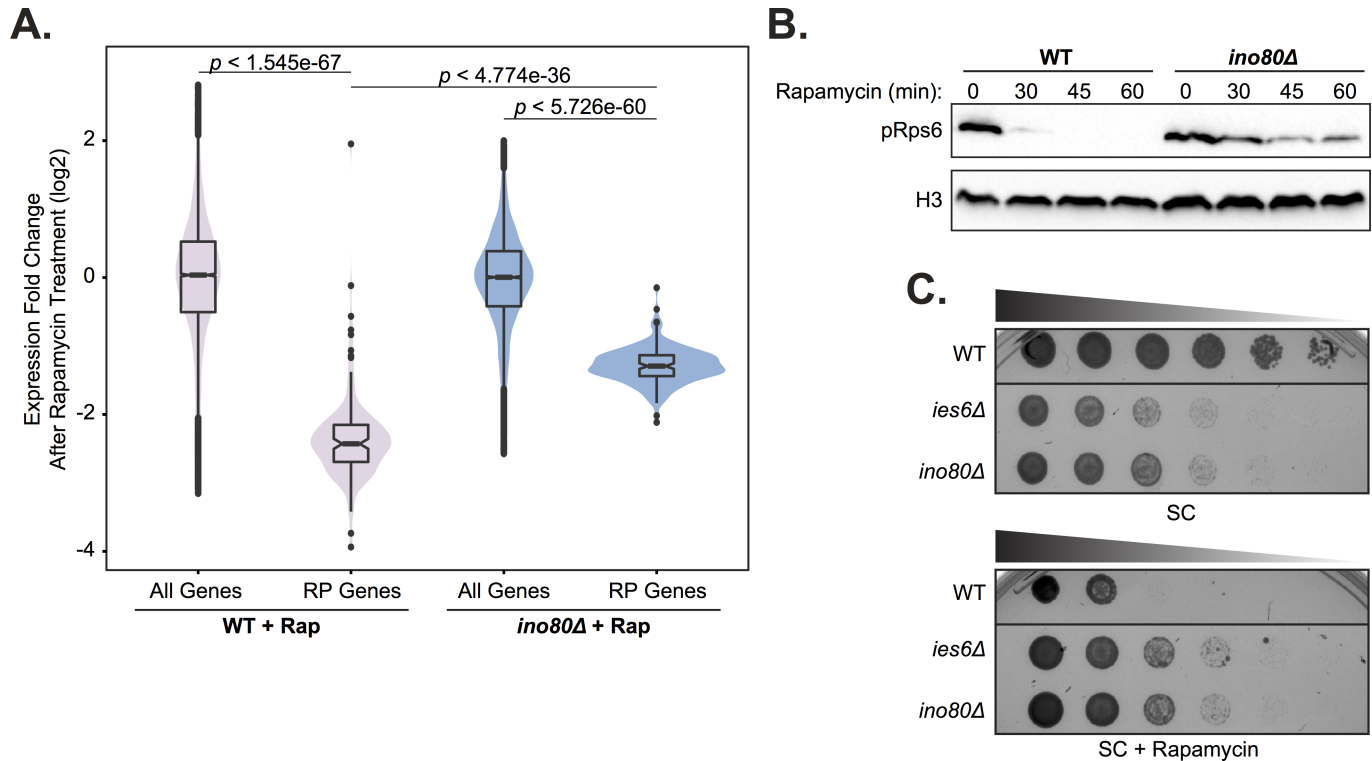
Fig 8. INO80 is an effector of the TORC1 pathway. (A) Violin and box plots of log-transformed expression fold-change after 45 minutes of 30 nM rapamycin (Rap) treatment compared to untreated cells in the indicated strains. The top and bottom 3% of genome wide responses were excluded for plotting. Significance was determined using a Wilcoxon rank sum test with all genes. **(B)** Western analysis of phospho-Rps6 (pRps6) reduction following 30 nM rapamycin treatment for indicated minutes (min) in wild-type (WT) and *ino80Δ* strain. Histone H3 (H3) is a loading control. **(C)** Fitness assay of deletion strains compared to wild-type (WT). Serial dilution (1:5) of strains were grown at 30˚C on synthetic complete (SC) media with 0 or 5nM rapamycin.

https://doi.org/10.1371/journal.pgen.1007216.g008

correlation with rapamycin-treated cells (S12 Fig). Loss of *INO80* mimics many gene expression effects of rapamycin treatment, albeit to a lesser degree, including nitrogen metabolism, Msn2/4 stress response genes, and ribosome biogenesis (Fig 7B and S8 Table). The expression of TORC1-responsive signaling and downstream transcription factors are similarly misregulated in both *ino80Δ* and rapamycin-treated cells.

We also observed that *ino80Δ* cells were much less responsive to rapamycin treatment, which may result from compensatory mechanisms that emerge as a result of constitutively diminished TORC1-mediated transcription. Specifically, following rapamycin treatment, TORC1-responsive ribosomal protein (RP) gene expression in *ino80Δ* mutants is not decreased to the same degree as in wild-type cells (Fig 8A). Additionally, TORC1-dependent phosphorylation of Rps6, a ribosome component, persists in *ino80Δ* mutants following rapamycin treatment (Fig 8B). We also found that in growth assays, *ies6Δ* and *ino80Δ* mutants are resistant to rapamycin treatment (Fig 8C). Collectively, these observations demonstrate that loss of INO80 function results in persistent inability to transmit TORC1 signaling to chromatin and the creation of rapamycin refractory cells.

Discussion

In this report, we examine an expansive genetic map to identify the functional composition of the INO80 complex. Unlike that of SWR1 unique subunits, the INO80 complex is genetically

diverse and partitioned among several distinct modules. Partial function of the INO80 complex is constrained within structural modules [22], such as the Nhp10 module, the subunits of which have cohesive genetic signatures. However, unexpected diversity is found with the Ies6 subunit, which forms a distinct genetic module that is anti-correlated with other INO80 subunits, including Arp5, its physical partner [18,22,23]. Interestingly, these unique Ies6 genetic interactions are enriched in metabolic functions and reveal previously unknown activities for the INO80 complex in mitochondrial maintenance and TOR signaling.

The role of Ino80 and Ies6 in mitochondrial inheritance (Fig 3D) may be indicative of a broader role for INO80 and/or Ies6 in the organization of organelles via the cytoskeleton. INO80 subunits genetically interact with genes involved in microtubule nucleation, actin cytoskeleton organization, and vesicle fusion (Fig 3B). Furthermore, in another genetic study, INO80 was connected to multivesicular body (MVB) sorting, cell polarity and morphogenesis, and cytokinesis [60].

Importantly, our genetic data has uncovered a strong connection between INO80 and TORC1, a rapamycin sensitive complex that is a master regulator of cell growth in yeast, plants and animals [40]. TORC1 signaling is active in nutrient rich conditions and promotes ribosome biogenesis while repressing cellular stress responses [61] (Fig 7B). INO80 and TORC1 have shared functions both in nutrient rich and rapamycin stress conditions, as indicated by correlated genetic profiles (Fig 4A and S2 Fig and S3 Fig) and direct genetic interactions between INO80 and the TORC1 signaling pathway (Fig 6 and S11 Fig). INO80 subunits are hub genes, that is highly connected nodes, in our rapamycin differential network, supporting a central role for INO80 in responding to rapamycin treatment. Additionally, similar transcriptional profiles are observed in *ino80Δ* mutants and cells treated with rapamycin (Fig 7A). Collectively, these data suggest that INO80 is needed to communicate TORC1-mediated growth signaling to chromatin.

One way in which INO80 can facilitate TORC1-dependent gene expression is by regulating histone acetylation status, thus transcriptional potential. Our study finds that INO80 genetically interacts with the acetyltransferases Rtt109 and SAGA, and with several rapamycin-responsive deacetylases, including Rpd3L and Hst3 (Fig 4A and 4B and Fig 5C). Interestingly, both Rpd3L and acetylated H3K56, the product of Rtt109 acetylation, are in the TORC1 signaling pathway [55,62,63]. The genome occupancy of Arp5 and acetylated H3K56 correlate, as do many histone acetyl marks, and loss of *INO80* reduces histone acetylation at metabolic loci (Fig 5A and 5E). Thus, INO80 may function to promote histone acetylation on growth genes downstream of TORC1 signaling.

Histone acetylation is also intimately linked to metabolic status, as it requires the metabolic intermediate acetyl-CoA. High levels of histone acetylation are present on genes that regulate the metabolome (Fig 5D and S8B Fig and S9A Fig), perhaps reflecting a feedback loop, whereby expression of metabolome regulators promotes acetyl-CoA production, which subsequently increases histone acetylation and gene expression. Thus, changes in metabolite availability could signal environmental conditions that are translated through chromatin. Future research will be needed to determine the role of INO80 and other chromatin remodelers that link metabolic status to epigenetic programming.

However, it is known that the consequences of deregulated metabolic signaling often result in disease. Indeed, energy metabolism alterations are a major contributing factor for many pathologies, including cancer, cardiovascular disease, and diabetes, which together account for two-thirds of all deaths in industrialized nations. For example, the mTOR signaling pathway is often constitutively active in cancer, promoting growth signaling irrespective of metabolic environments [64]. In this study, we find that the INO80 complex is needed to enact TORC1-responsive transcriptional programs. As both TORC1 and INO80 are conserved from yeast to humans, we
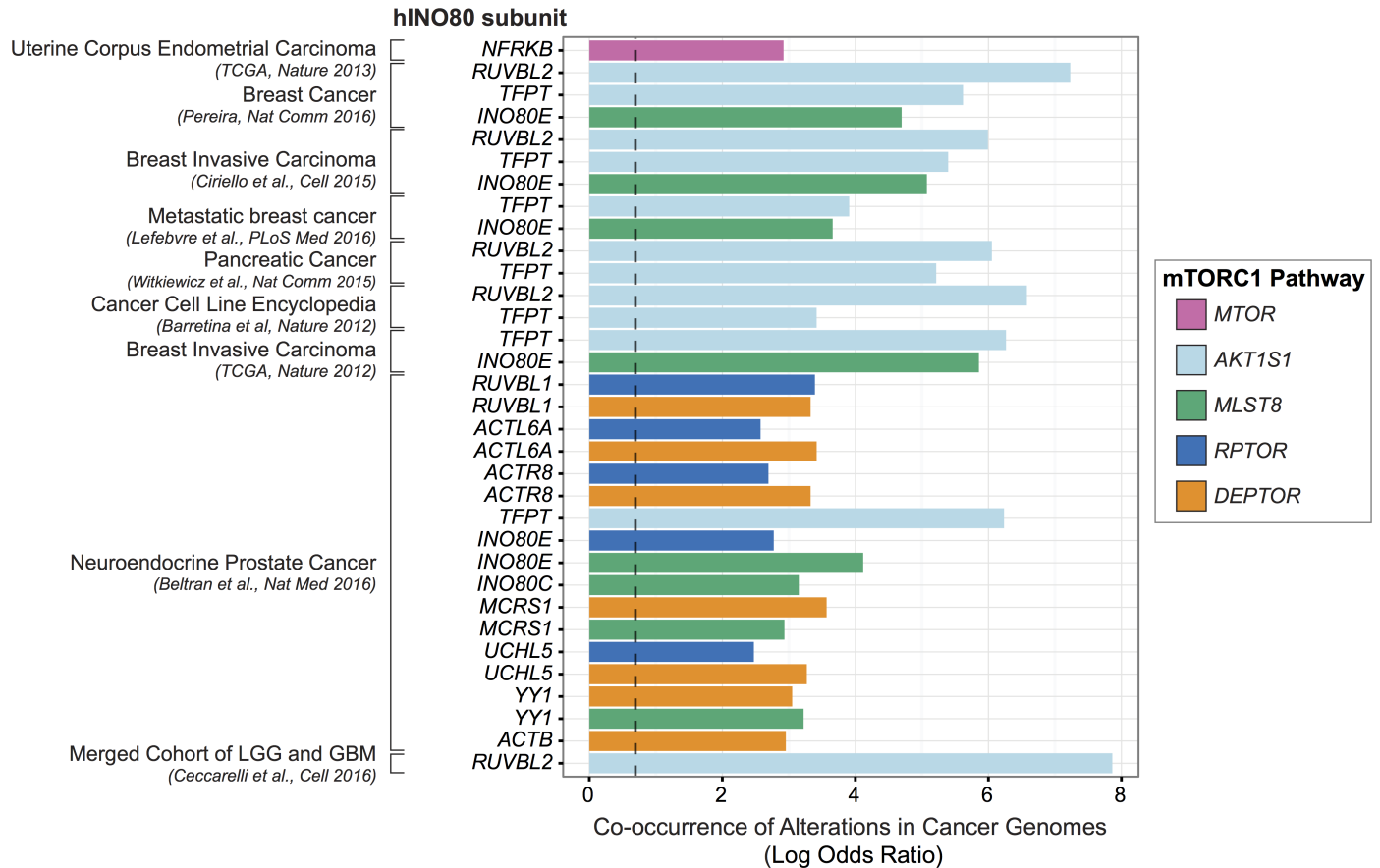
Fig 9. INO80 and mTORC1 alterations co-occur in cancers. Co-occurrence of INO80 subunit and mTORC1 alteration in cancer using datasets [80–99] from the cBioPortal [100–102]. Datasets with high mutational load in the INO80/mTOR pathway gene sets (>20% altered samples) were used and small (< 50 samples) and provisional datasets were excluded. The natural log transformed odds ratio calculated by the mutual exclusivity tool in the portal is plotted for significant co-occurrences (Fisher's Exact Test and false discovery rate of 0.001). Infinite calculated odds ratios are excluded. The dashed line marks tendency for co-occurrence (odds ratio of 2). Colors indicate mTORC1 subunits, human INO80 subunits are on the y-axis, co-occurrences are grouped by cancer study. The full table of significant co-occurrences is found in S9 Table.

https://doi.org/10.1371/journal.pgen.1007216.g009

investigated overlapping mutational signatures in cancer patient datasets. Indeed, we observed a high co-occurrence of alterations in subunits of hINO80 and mTORC1 in a wide range of human cancers (Fig 9 and S9 Table), suggesting that abrogation of both INO80 and mTORC1 may lead to the metabolic dysregulation that contributes to carcinogenesis.

INO80, like many chromatin remodelers, has numerous roles in DNA-templated processes. Investigations of how these remodelers are controlled will likely reveal how chromatin modification is integrated with environmental responses. In this report, we have identified that the functions of the INO80 complex are modular, thus may be regulated in parts, rather than affecting the totality of INO80's activity. Furthermore, we reveal that INO80 is involved in metabolic signaling, which likely contributes to adaptive gene expression responses in normal cells and may result in disease when disrupted.

Materials and methods

Differential genetic interaction screens

Genetic interaction screens (EMAPs) were performed as described [65] except that the last selection step was performed by replica-plating cells on medium containing YPD

(untreated), 10nM Rapamycin on SC, or YPD lacking glucose and containing 2% ethanol. Images for score calculations were taken 24 hours after pinning except for ethanol which was taken 48 hours afterwards. Static and differential genetic interaction scores were calculated using a MATLAB-based software toolbox as described [38,43] using standard significance thresholds for the static conditions (S ≥ 2.0 or S ≤ -2.5) and the differential conditions (S ≥ 3.0 or S ≤ -3.0).

Yeast strains

Yeast strains are listed in S10 Table. Strain construction was in S288C background using standard techniques. All FLAG epitopes were chromosomally integrated to ensure endogenous expression of protein. Gene deletions were integrated at the chromosomal locus.

The EMAP query strains are haploid Matα yeast, as in [65], containing NAT marked mutations with the following background genotype: *his3Δ1 leu2Δ0 LYS2+ met15Δ0 ura3Δ0 can1Δ:: MATa STE2Pr-HIS3 lyp1Δ::MATα STE3Pr-LEU2*. The EMAP test strains are haploid Mat*a* yeast, as in [42], containing KAN[R] marked mutations with the following background genotype: *his3Δ1 leu2Δ0 met15Δ0 ura3Δ0*. *D*ecreased *a*bundance by *m*RNA *p*erturbation (DAmP) alleles are as previously described [36].

INO80 subunit domain mutants

The following domain mutants of Ino80, Arp5, and Ies6 were used in this study. For the Ino80 ATPase subunit that scaffolds the complex, we deleted 3 domains: amino acids 2–200 (N-terminus, Nterm), which is required for association of the Nhp10 module (Ies1, Ies3, Nhp10, Ies5); the helicase-SANT-associated (HSA) domain [44] required for association of the Arp8 module (Arp8, Arp4, Act1, Ies4); and the insertion domain that splits Ino80's two RecA ATPase lobes and is required for association of the Arp5 and Rvb1/2 modules (Arp5, Ies6, Ies2, Rvb1, Rvb2) [30]. Two previously described domain mutants of the Arp5 subunit that are conserved across species but unique to Arp5 and help couple ATPase activity to productive nucleosome sliding [30] were used (D2 and D3).

For the Ies6 subunit that is a component of the Arp5 module [30], domain deletions across *IES6* based on conservation, hydrophobicity, intrinsic disorder, and protein interactions were created. We individually deleted two regions of the YL1-C domain, which is needed for the Arp6-Ies6 subcomplex to associate with INO80 [30]. The C-terminal deletion (D5) strain was viable but EMAP results from this query did not pass quality control analysis and were subsequently excluded, while the N-terminal deletion (D4) query produced consistent EMAP results.

Domain mutants contain a C-terminal selectable marker after 500bp of endogenous 3' sequence, except for the Swc2-YL1C*Δ* (AA 708–737*Δ*) mutant which has 449bp of 3' sequence, and the Ino80-Nterm domain mutant, which contains a selectable marker 700bp upstream of the ORF, followed by endogenous 5' sequence.

Western blotting

Protein from whole cell extracts were precipitated with 10% trichloroacetic acid. Proteins were detected by Western blot using anti-FLAG M2 (Sigma; catalog no. F1804), anti-hexokinase (Novus; catalog no. NB120-20547), anti-H3 C-terminal (Active Motif; catalog no. 39163), or anti-phospho-S6 ribosomal protein (Cell Signaling Technology; catalog no. 2211) antibodies. Blots are representative of at least three biological replicates.

FLAG affinity purifications

Protein complexes were purified using FLAG affinity-agarose beads (Sigma; catalog no. A2220) as previously described [30], and washed with HEGN buffer containing 0.5M KCl.

Bioinformatic analysis

Bioinformatic analysis was conducted using R. Rankit normalization was performed on ranked values using the formula (r– 0.5) /n across a normal distribution [66]. Pearson correlations were performed using the cor() function, principal component analyses were performed using the prcomp() function. Genetic modules were determined using hierarchical clustering along with the kmeans() clustering algorithm. The number of centers was informed with a combination of a within sum of squares plot, average silhouette approach, and a gap statistic plot using the 'factoextra' R package, as well as a rational approach incorporating published structural data of the complex. The Benjamini & Hochberg method was used for multiple test correction using p.adjust().

DAVID analysis was performed using version 6.7 with default parameters and medium stringency. Gene ontology (GO) enrichments were determined from GO annotations retrieved using the org.Sc.sgd.db R package (Bioconductor) after applying a multiple hypothesis corrected hypergeometric test using genes in the EMAP test library as background with a custom script.

Genome wide ChIP-seq correlations were performed using the Genome Track Analyzer [67] on uniformly processed tracks using segment midpoints and considering both strands. The H3K56ac and Arp5 correlation reported in the text (r = 0.53) was calculated from uniformly processed data using the multiBigwigSummary and plotCorrelation tools in the deep-Tools2 suite [68] using 10 bp bins and Pearson correlation. Arp5 and H3K18ac occupancy profiles were generated from averaged ChIP traces ±1 kb around the +1 nucleosomes of all ORFs, smoothed by fitting a spline function selected by ordinary cross-validation in R using smooth.spline(), then scaled and centered using the scale() function in R.

Network density was calculated as number of significant interactions observed divided by the total number of query-test gene pairs. Significance for network densities was assessed using a Monte Carlo randomization test. Randomization tests were performed with 100,000 permutations. Significance is notated as follows: * $p < .05$, ** $p < .01$, *** $p < .001$, n.s. is not significant.

Petite frequency assay

Petite frequency was measured as previously described using a tetrazolium overlay [52].

RNA-sequencing

RNA was prepared from samples (approximately 1.5 ODs) in biological duplicate using the MasterPure Yeast RNA Purification Kit (Epicentre, MPY03100). The sequencing libraries were prepared from 0.8 μg of RNA/sample using the Illumina TruSeq Stranded mRNA kit (Illumina, 15031047). The quality of the pooled library was checked using the Agilent Bioanalyser 2100 HS DNA assay. The library was sequenced on an Illumina HiSeq 2000 platform. Minimum of 10 million reads per sample were aligned using Bowtie 2 and analyzed using the DESeq2 package for R. Data available under NCBI accession GSE103468.

Uniform ChIP-seq processing

Reads were downloaded from GEO and uniformly processed. Briefly, reads were truncated to the smallest read length across datasets (36bp), mapped to the genome using STAR, and then

signal coverage was generated and peaks were called using MACS2. Uniform processing of ChIP-seq data facilitates inter-study comparisons and can eliminate batch artifacts. Datasets used [7,69–75] are listed in S5 Table. +1 nucleosome positions were used as defined in [76]. Datasets of insufficient quality after processing were excluded from subsequent analysis.

ChIP-qPCR

ChIP was performed as previously described [45] with a few modifications. Cells were grown in YPD at 30˚C to OD_{660} of 0.7. Cells were lysed using Matrix D beads in a FastPrep homogenizer (MP Biomedicals) at maximum four times for 60 seconds, then sonicated to an average fragment size of 300 bp using a Bioruptor Plus (Diagenode) and clarified by centrifugation. Chromatin was immunoprecipitated using anti-H3K18ac (Millipore; catalog no. 07–354) prebound to Protein G Dynabeads (ThermoFisher; catalog no. 10004D) and washed 3 times in FA buffer with 150 mM NaCl then 2 times in FA buffer with 500 mM NaCl. DNA was eluted in TE with 1% SDS, cross-links were reversed by incubating overnight at 65˚C, treated with 0.2mg/ml RNAse A (VWR; catalog no. E866) for 2 hours at 37˚C, then extracted with phenol: chloroform:isoamylalchol and ethanol precipitated. DNA was resuspended in TE and analyzed by real-time quantitative PCR using iTaq Universal SYBR Green Supermix (BioRad; catalog no. 1725121). Ct values were determined using a CFX96 real-time detection system (BioRad).

Supporting information

S1 Fig. Ies6 and Ino80 domain mutants created for this study. (A) Schematic of the Ino80 ATPase protein domains with subunit binding modules illustrated from previous structural and biochemical studies [22,30]. Ino80 insertion is as described by [103], HSA domain is as identified in [44], N-terminus (Nterm) is amino acids 2–200. **(B)** Ino80-FLAG purifications from wild-type (WT), N-terminal deletion (Nterm), and HSA deletion strains were electrophoresed on 6% (top) and 15% (bottom) SDS-PAGE gels and identified by asterisk. Proteins were visualized via silver staining. Subunits of the INO80 complex are labeled on the right, molecular mass (KDa) is labeled on the left. Subunits lost from the INO80 complex are identified at the bottom. **(C)** Schematic of Ies6 gene domains, the YL1-C domain is split into domain 4 (D4) and domain 5 (D5). D5 was omitted from additional assays because EMAP results did not pass quality control (QC). **(D)** Fitness assay of indicated FLAG-tagged domain mutants described in (C). 1:10 serial dilution of strains were grown for 3 days at 30˚C on YPD. (PDF)

S2 Fig. Hierarchical clustering of genetic interaction scores in untreated condition. Clustergram of all significant interactions in the untreated static EMAP between the 54 query strains and all test strains with at least one significant interaction. Test strains are along the x-axis. Text colors correspond to the query category annotated in Fig 1B. S1 Table lists all EMAP scores. (PDF)

S3 Fig. Hierarchical clustering of genetic interaction scores in the rapamycin differential condition. Clustergram of all significant interactions in the rapamycin differential EMAP between the 54 query strains and all test strains with at least one significant interaction. Test strains are along the x-axis. Text colors correspond to the query category annotated in Fig 1B. S1 Table lists all EMAP scores. (PDF)

S4 Fig. Hierarchical clustering of genetic interaction scores in the ethanol differential condition. Clustergram of all significant interactions in the ethanol differential EMAP between

the 54 query strains and all test strains with at least one significant interaction. Test strains are along the x-axis. Text colors correspond to the query category annotated in Fig 1B. S1 Table lists all EMAP scores.
(PDF)

S5 Fig. Significant interactions in the ethanol differential network. Plot of normalized significant interactions by query gene in the untreated condition and the ethanol differential condition, as in Fig 1F.
(PDF)

S6 Fig. Genetic organization of INO80 and SWR1 in rapamycin and ethanol. Heatmap illustrating pairwise Pearson correlations between INO80 (**A-D**) and SWR1 (**E-H**) complex subunit query strains across the test library, as in Fig 2A and 2B. Rapamycin static correlations (**A** and **E**) and differential correlations (**B** and **F**) are shown. Ethanol static correlations (**C** and **G**) and differential correlations (**D** and **E**) are shown. Strains are ordered as shown in Fig 2A and 2B and determined by untreated hierarchical clustering.
(PDF)

S7 Fig. Genetic organization of the INO80 subfamily of remodeling complexes. (A) Heatmap of Pearson correlation of INO80 and SWR1 complex subunit query strains in the untreated static condition, as in Fig 2A; colors delineate complexes as in Fig 1B. Mutants are complete deletions or domain deletions where indicated: *INO80* N-terminal (NTERM), insertion (INS), and HSA deletions; *ARP5* domain 2 and 3 (D2 and D3) deletions; and *IES6* domain 1, 2, 3, 4, and 6 (D1, D2, D3, D4, D6) deletions. *D*ecreased *a*bundance by *m*RNA *p*erturbation (DAmP) alleles are as described in [36]. Boxes outline subunit clusters identified by hierarchical clustering. **(B)** Principal component analysis (PCA) of INO80 and SWR1 complex subunit query strain Pearson correlations, as in Fig 2B. Colors indicate clusters identified by k-means clustering (k = 3).
(PDF)

S8 Fig. H3K18ac genome occupancy profile. (A) Genome-wide average uniformly processed (see *Materials and Methods*) ChIP-seq levels ±1000 bp from +1 nucleosomes [76] of Arp5 [7] and H3K18ac [69]. **(B)** Genes with high H3K18ac levels at +1 nucleosomes are significantly enriched for regulators of the metabolome; significance was determined using a hypergeometric test.
(PDF)

S9 Fig. Histone modifications correlate with one another at +1 nucleosomes. (A) Heatmap of pairwise squared Pearson correlations at +1 nucleosomes using uniformly processed published ChIP-seq data (see *Materials and Methods*). Modifications that have significantly high levels at the +1 nucleosomes of metabolome regulators and are enriched for metabolome regulators in their top quartile of +1 nucleosome levels are bolded. **(B)** Box and jittered scatter plots of correlations between all histone marks shown and the metabolome enriched marks bolded in (A). Significance is determined using a Wilcoxon rank sum test ($p < 4.1e-4$) and by Monte Carlo randomization test ($p = 0.0419$).
(PDF)

S10 Fig. IES6 clusters in a rapamycin-sensitive metabolic module. (A) Table showing select gene ontology (GO) terms enriched in test strains that significantly interact with the IES6 cluster query genes (FDR-adjusted hypergeometric test, $p < .05$). The complete list of significant GO terms is found in S7 Table. **(B)** Box and jittered scatter plots of correlations between query genes in the INO80 and IES6 expanded modules, shown in Fig 4A, in the untreated static,

rapamycin static and differential conditions. Significance is determined using a Wilcoxon rank sum test.
(PDF)

S11 Fig. INO80 and the TOR pathway are highly connected in the rapamycin EMAP. Genetic interaction network between INO80 subunit query strains and significantly interacting TOR pathway test strains in the rapamycin differential condition. Line width indicates strength of S-score, INO80 queries are colored according to modules identified in Fig 2. Network density is significantly high, *p*-value = 1.6e-4 by Monte Carlo randomization test.
(PDF)

S12 Fig. Ies2 mutants transcriptionally correlate with rapamycin-treated cells. Log-transformed Z-scores of expression fold-change between untreated and treated wild-type cells or indicated deletion strains representing the top 5 highest correlating samples to rapamycin treatment from Urban *et al.* 2007 [54,59,104]. Genes with at least a Z-score of ±1.0 are plotted. Pearson correlations are shown for all genes (>5800) regardless of fold-change difference.
(PDF)

S1 Table. Genetic interaction data generated by static and differential EMAPs.
(XLSX)

S2 Table. Significant query interactions by treatment.
(XLSX)

S3 Table. DAVID functional annotation clusters by module.
(XLSX)

S4 Table. Gene ontology enrichments by module.
(XLSX)

S5 Table. ChIP-seq datasets uniformly processed for analysis in this study.
(XLSX)

S6 Table. Network density of histone acetyl transferases and INO80 interactions.
(XLSX)

S7 Table. Gene ontology enrichments of the expanded IES6 genetic module.
(XLSX)

S8 Table. Lists of genes in pathways utilized in this study.
(XLSX)

S9 Table. Mutual exclusivity data generated by cBioPortal for INO80 and mTORC1 subunits.
(XLSX)

S10 Table. List of yeast strains used. (**A**) Yeast strains used in this study. (**B**) EMAP query strains used in this study. (**C**) EMAP test strains used in this study.
(XLSX)

Acknowledgments

Author Contributions

Conceptualization: Sean L. Beckwith, Ashby J. Morrison.

Formal analysis: Sean L. Beckwith, Pablo E. García-Nieto, Devin A. King, Graeme J. Gowans.

Funding acquisition: Ashby J. Morrison.

Investigation: Sean L. Beckwith, Erin K. Schwartz, Pablo E. García-Nieto, Devin A. King, Graeme J. Gowans, Ka Man Wong, Tessa L. Eckley, Wei Yao, Ashby J. Morrison.

Project administration: Erin K. Schwartz, Ashby J. Morrison.

Resources: Sean L. Beckwith, Tessa L. Eckley, Alexander P. Paraschuk, Egan L. Peltan, Laura R. Lee.

Software: Sean L. Beckwith, Pablo E. García-Nieto, Devin A. King.

Supervision: Ashby J. Morrison.

Validation: Sean L. Beckwith.

Visualization: Sean L. Beckwith.

Writing – original draft: Sean L. Beckwith, Ashby J. Morrison.

Writing – review & editing: Sean L. Beckwith, Ashby J. Morrison.

References

1. Clapier CR, Cairns BR. The biology of chromatin remodeling complexes. Annu Rev Biochem. 2009; 78: 273–304. https://doi.org/10.1146/annurev.biochem.77.062706.153223 PMID: 19355820

2. Davis P, Brachmann R. Chromatic Remodeling and Cancer. Cancer Biol Ther. 2003; 2: 24–31. Available: http://www.landesbioscience.com/journals/cbt/davis2-1.pdf?origin=publication_detail

3. de la Serna IL, Ohkawa Y, Imbalzano AN. Chromatin remodelling in mammalian differentiation: lessons from ATP-dependent remodellers. Nat Rev Genet. 2006; 7: 461–73. https://doi.org/10.1038/nrg1882 PMID: 16708073

4. Wu JI. Diverse functions of ATP-dependent chromatin remodeling complexes in development and cancer. Acta Biochim Biophys Sin (Shanghai). 2012; 44: 54–69. https://doi.org/10.1093/abbs/gmr099.Review

5. Alcid E a., Tsukiyama T. ATP-dependent chromatin remodeling shapes the long noncoding RNA landscape. Genes Dev. 2014; 28: 2348–2360. https://doi.org/10.1101/gad.250902.114 PMID: 25367034

6. Shen X, Mizuguchi G, Hamiche a, Wu C. A chromatin remodelling complex involved in transcription and DNA processing. Nature. 2000; 406: 541–4. https://doi.org/10.1038/35020123 PMID: 10952318

7. Xue Y, Van C, Pradhan SK, Su T, Gehrke J, Kuryan BG, et al. The Ino80 complex prevents invasion of euchromatin into silent chromatin. Genes Dev. 2015; 29: 350–355. https://doi.org/10.1101/gad.256255.114 PMID: 25691465

8. Papamichos-Chronakis M, Peterson CL. The Ino80 chromatin-remodeling enzyme regulates replisome function and stability. Nat Struct Mol Biol. 2008; 15: 338–45. https://doi.org/10.1038/nsmb.1413 PMID: 18376411

9. Shimada K, Oma Y, Schleker T, Kugou K, Ohta K, Harata M, et al. Ino80 chromatin remodeling complex promotes recovery of stalled replication forks. Curr Biol. 2008; 18: 566–75. https://doi.org/10.1016/j.cub.2008.03.049 PMID: 18406137

10. Vincent J a, Kwong TJ, Tsukiyama T. ATP-dependent chromatin remodeling shapes the DNA replication landscape. Nat Struct Mol Biol. 2008; 15: 477–84. https://doi.org/10.1038/nsmb.1419 PMID: 18408730

11. Attikum H Van, Fritsch O, Hohn B, Gasser SM, Ansermet QE, Geneva C-. Recruitment of the INO80 Complex by H2A Phosphorylation Links ATP-Dependent Chromatin Remodeling with DNA Double-Strand Break Repair NCCR Frontiers in Genetics Program. Cell. 2004; 119: 777–788. https://doi.org/10.1016/j.cell.2004.11.033 PMID: 15607975

12. Morrison AJ, Kim J-A, Person MD, Highland J, Xiao J, Wehr TS, et al. Mec1/Tel1 phosphorylation of the INO80 chromatin remodeling complex influences DNA damage checkpoint responses. Cell. 2007; 130: 499–511. https://doi.org/10.1016/j.cell.2007.06.010 PMID: 17693258

13. Morrison AJ, Highland J, Krogan NJ, Arbel-Eden A, Greenblatt JF, Haber JE, et al. INO80 and γ-H2AX interaction links ATP-dependent chromatin remodeling to DNA damage repair. Cell. 2004; 119: 767–75. https://doi.org/10.1016/j.cell.2004.11.037 PMID: 15607974

14. Falbo KB, Alabert C, Katou Y, Wu S, Han J, Wehr T, et al. Involvement of a chromatin remodeling complex in damage tolerance during DNA replication. Nat Struct Mol Biol. 2009; 16: 1167–1172. https://doi.org/10.1038/nsmb.1686 PMID: 19855395

15. Yu EY, Steinberg-Neifach O, Dandjinou AT, Kang F, Morrison AJ, Shen X, et al. Regulation of telomere structure and functions by subunits of the INO80 chromatin remodeling complex. Mol Cell Biol. 2007; 27: 5639–49. https://doi.org/10.1128/MCB.00418-07 PMID: 17562861

16. Chambers AL, Ormerod G, Durley SC, Sing TL, Brown GW, Kent N a, et al. The INO80 chromatin remodeling complex prevents polyploidy and maintains normal chromatin structure at centromeres. Genes Dev. 2012; 26: 2590–603. https://doi.org/10.1101/gad.199976.112 PMID: 23207916

17. Ogiwara H, Enomoto T, Seki M. The INO80 Chromatin Remodeling Complex Functions in Sister Chromatid Cohesion. Cell Cycle. 2007; 6: 1090–1095. https://doi.org/10.4161/cc.6.9.4130 PMID: 17471029

18. Yao W, King DA, Beckwith SL, Gowans GJ, Yen K, Zhou C, et al. The INO80 Complex Requires the Arp5-Ies6 Subcomplex for Chromatin Remodeling and Metabolic Regulation. Mol Cell Biol. 2016; 36: 979–91. https://doi.org/10.1128/MCB.00801-15 PMID: 26755556

19. Morrison AJ. Genome maintenance functions of the INO80 chromatin remodeller. Philos Trans R Soc B Biol Sci. 2017; 372: 20160289. https://doi.org/10.1098/rstb.2016.0289 PMID: 28847826

20. Morrison AJ, Shen X. Chromatin remodelling beyond transcription: the INO80 and SWR1 complexes. Nat Rev Mol Cell Biol. 2009; 10: 373–84. https://doi.org/10.1038/nrm2693 PMID: 19424290

21. Poli J, Gasser SM, Papamichos-Chronakis M. The INO80 remodeller in transcription, replication and repair. Philos Trans R Soc B Biol Sci. 2017; 372: 20160290. https://doi.org/10.1098/rstb.2016.0290 PMID: 28847827

22. Tosi A, Haas C, Herzog F, Gilmozzi A, Berninghausen O, Ungewickell C, et al. Structure and Subunit Topology of the INO80 Chromatin Remodeler and Its Nucleosome Complex. Cell. Elsevier Inc.; 2013; 154: 1207–1219. https://doi.org/10.1016/j.cell.2013.08.016 PMID: 24034245

23. Watanabe S, Tan D, Lakshminarasimhan M, Washburn MP, Erica Hong E-J, Walz T, et al. Structural analyses of the chromatin remodelling enzymes INO80-C and SWR-C. Nat Commun. Nature Publishing Group; 2015; 6: 7108. https://doi.org/10.1038/ncomms8108 PMID: 25964121

24. Gerhold CB, Winkler DD, Lakomek K, Seifert FU, Fenn S, Kessler B, et al. Structure of Actin-related protein 8 and its contribution to nucleosome binding. Nucleic Acids Res. 2012; 40: 11036–46. https://doi.org/10.1093/nar/gks842 PMID: 22977180

25. Harata M, Oma Y, Mizuno S, Jiang YW, Stillman DJ, Wintersberger U. The nuclear actin-related protein of Saccharomyces cerevisiae, Act3p/Arp4, interacts with core histones. Mol Biol Cell. 1999; 10: 2595–605. PMID: 10436015

26. Kapoor P, Chen M, Winkler DD, Luger K, Shen X. Evidence for monomeric actin function in INO80 chromatin remodeling. Nat Struct Mol Biol. 2013; 20: 426–32. https://doi.org/10.1038/nsmb.2529 PMID: 23524535

27. Saravanan M, Wuerges J, Bose D, McCormack E a, Cook NJ, Zhang X, et al. Interactions between the nucleosome histone core and Arp8 in the INO80 chromatin remodeling complex. Proc Natl Acad Sci U S A. 2012; 109: 20883–8. https://doi.org/10.1073/pnas.1214735109 PMID: 23213201

28. Shen X, Ranallo R, Choi E, Wu C. Involvement of actin-related proteins in ATP-dependent chromatin remodeling. Mol Cell. 2003; 12: 147–55. PMID: 12887900

29. Jin J, Cai Y, Yao T, Gottschalk AJ, Florens L, Swanson SK, et al. A mammalian chromatin remodeling complex with similarities to the yeast INO80 complex. J Biol Chem. 2005; 280: 41207–12. https://doi.org/10.1074/jbc.M509128200 PMID: 16230350

30. Yao W, Beckwith SL, Zheng T, Young T, Dinh VT, Ranjan A, et al. Assembly of the Arp5 (Actin-related Protein) Subunit Involved in Distinct INO80 Chromatin Remodeling Activities. J Biol Chem. 2015; 290: 25700–9. https://doi.org/10.1074/jbc.M115.674887 PMID: 26306040

31. Gut P, Verdin E. The nexus of chromatin regulation and intermediary metabolism. Nature. 2013; 502: 489–498. https://doi.org/10.1038/nature12752 PMID: 24153302

32. Shi L, Tu BP. Acetyl-CoA and the regulation of metabolism: mechanisms and consequences. Curr Opin Cell Biol. Elsevier Ltd; 2015; 33: 125–131. https://doi.org/10.1016/j.ceb.2015.02.003 PMID: 25703630

33. Murayama A, Ohmori K, Fujimura A, Minami H, Yasuzawa-Tanaka K, Kuroda T, et al. Epigenetic Control of rDNA Loci in Response to Intracellular Energy Status. Cell. 2008; 133: 627–639. https://doi.org/10.1016/j.cell.2008.03.030 PMID: 18485871

34. Zhou CY, Johnson SL, Gamarra NI, Narlikar GJ. Mechanisms of ATP-Dependent Chromatin Remodeling Motors. Annu Rev Biophys. 2016; 45: 153–181. https://doi.org/10.1146/annurev-biophys-051013-022819 PMID: 27391925

35. Beltrao P, Cagney G, Krogan NJ. Quantitative genetic interactions reveal biological modularity. Cell. 2010; 141: 739–45. https://doi.org/10.1016/j.cell.2010.05.019 PMID: 20510918

36. Schuldiner M, Collins SR, Thompson NJ, Denic V, Bhamidipati A, Punna T, et al. Exploration of the function and organization of the yeast early secretory pathway through an epistatic miniarray profile. Cell. 2005; 123: 507–19. https://doi.org/10.1016/j.cell.2005.08.031 PMID: 16269340

37. Collins SR, Miller KM, Maas NL, Roguev A, Fillingham J, Chu CS, et al. Functional dissection of protein complexes involved in yeast chromosome biology using a genetic interaction map. Nature. 2007; 446: 806–810. https://doi.org/10.1038/nature05649 PMID: 17314980

38. Bandyopadhyay S, Mehta M, Kuo D, Sung K, Chuang R, Jaehnig EJ, et al. Rewiring of genetic networks in response to DNA damage. Science (80-). 2010; 330: 1385–1389. https://doi.org/10.1126/science.1195618 PMID: 21127252

39. Guénolé A, Srivas R, Vreeken K, Wang ZZ, Wang S, Krogan NJ, et al. Dissection of DNA Damage Responses Using Multiconditional Genetic Interaction Maps. Mol Cell. 2013; 49: 346–358. https://doi.org/10.1016/j.molcel.2012.11.023 PMID: 23273983

40. Loewith R, Hall MN. Target of Rapamycin (TOR) in Nutrient Signaling and Growth Control. Genetics. 2011; 189: 1177–1201. https://doi.org/10.1534/genetics.111.133363 PMID: 22174183

41. Zaman S, Lippman SI, Zhao X, Broach JR. How Saccharomyces responds to nutrients. Annu Rev Genet. 2008; 42: 27–81. https://doi.org/10.1146/annurev.genet.41.110306.130206 PMID: 18303986

42. Ryan CJ, Roguev A, Patrick K, Xu J, Jahari H, Tong Z, et al. Hierarchical Modularity and the Evolution of Genetic Interactomes across Species. Mol Cell. 2012; 46: 691–704. https://doi.org/10.1016/j.molcel.2012.05.028 PMID: 22681890

43. Collins SR, Schuldiner M, Krogan NJ, Weissman JS. A strategy for extracting and analyzing large-scale quantitative epistatic interaction data. Genome Biol. 2006; 7: R63. https://doi.org/10.1186/gb-2006-7-7-r63 PMID: 16859555

44. Szerlong H, Hinata K, Viswanathan R, Erdjument-Bromage H, Tempst P, Cairns BR. The HSA domain binds nuclear actin-related proteins to regulate chromatin-remodeling ATPases. Nat Struct Mol Biol. 2008; 15: 469–76. https://doi.org/10.1038/nsmb.1403 PMID: 18408732

45. Mizuguchi G, Shen X, Landry J, Wu W-H, Sen S, Wu C. ATP-driven exchange of histone H2AZ variant catalyzed by SWR1 chromatin remodeling complex. Science. 2004; 303: 343–8. https://doi.org/10.1126/science.1090701 PMID: 14645854

46. Nguyen VQ, Ranjan A, Stengel F, Wei D, Aebersold R, Wu C, et al. Molecular Architecture of the ATP-Dependent Chromatin-Remodeling Complex SWR1. Cell. The Authors; 2013; 154: 1220–1231. https://doi.org/10.1016/j.cell.2013.08.018 PMID: 24034246

47. Gerhold CB, Gasser SM. INO80 and SWR complexes: relating structure to function in chromatin remodeling. Trends Cell Biol. Elsevier Ltd; 2014; 1–13. https://doi.org/10.1016/j.tcb.2014.06.004 PMID: 25088669

48. Yen K, Vinayachandran V, Pugh BF. SWR-C and INO80 Chromatin Remodelers Recognize Nucleosome-free Regions Near +1 Nucleosomes. Cell. Elsevier Inc.; 2013; 154: 1246–1256. https://doi.org/10.1016/j.cell.2013.08.043 PMID: 24034248

49. Huang DW, Sherman BT, Lempicki RA. Bioinformatics enrichment tools: paths toward the comprehensive functional analysis of large gene lists. Nucleic Acids Res. 2009; 37: 1–13. https://doi.org/10.1093/nar/gkn923 PMID: 19033363

50. Huang DW, Sherman BT, Lempicki RA. Systematic and integrative analysis of large gene lists using DAVID bioinformatics resources. Nat Protoc. 2009; 4: 44–57. https://doi.org/10.1038/nprot.2008.211 PMID: 19131956

51. Hur S-K, Park E-J, Han J-E, Kim Y-A, Kim J-D, Kang D, et al. Roles of human INO80 chromatin remodeling enzyme in DNA replication and chromosome segregation suppress genome instability. Cell Mol Life Sci. 2010; 67: 2283–2296. https://doi.org/10.1007/s00018-010-0337-3 PMID: 20237820

52. Hess DC, Myers C, Huttenhower C, Hibbs MA, Hayes AP, Paw J, et al. Computationally driven, quantitative experiments discover genes required for mitochondrial biogenesis. PLoS Genet. 2009; 5. https://doi.org/10.1371/journal.pgen.1000407 PMID: 19300474

53. Watanabe S, Radman-Livaja M, Rando OJ, Peterson CL. A histone acetylation switch regulates H2A.Z deposition by the SWR-C remodeling enzyme. Science. 2013; 340: 195–9. https://doi.org/10.1126/science.1229758 PMID: 23580526

54. Lenstra TL, Benschop JJ, Kim T, Schulze JM, Brabers NACH, Margaritis T, et al. The Specificity and Topology of Chromatin Interaction Pathways in Yeast. Mol Cell. Elsevier Inc.; 2011; 42: 536–549. https://doi.org/10.1016/j.molcel.2011.03.026 PMID: 21596317

55. Humphrey EL, Shamji AF, Bernstein BE, Schreiber SL. Rpd3p Relocation Mediates a Transcriptional Response to Rapamycin in Yeast. Chem Biol. 2004; 11: 295–299. https://doi.org/10.1016/j.chembiol. 2004.03.001 PMID: 15123258

56. Rohde JR, Cardenas ME. The Tor Pathway Regulates Gene Expression by Linking Nutrient Sensing to Histone Acetylation. Mol Cell Biol. 2003; 23: 629–635. https://doi.org/10.1128/MCB.23.2.629-635. 2003 PMID: 12509460

57. Workman JJ, Chen H, Laribee RN. Saccharomyces cerevisiae TORC1 Controls Histone Acetylation by Signaling Through the Sit4/PP6 Phosphatase to Regulate Sirtuin Deacetylase Nuclear Accumulation. Genetics. 2016; 203: 1733–1746. https://doi.org/10.1534/genetics.116.188458 PMID: 27343235

58. Mülleder M, Calvani E, Alam MT, Wang RK, Eckerstorfer F, Zelezniak A, et al. Functional Metabolomics Describes the Yeast Biosynthetic Regulome. Cell. 2016; 1–13. https://doi.org/10.1016/j.cell. 2016.09.007 PMID: 27693354

59. Urban J, Soulard A, Huber A, Lippman S, Mukhopadhyay D, Deloche O, et al. Sch9 Is a Major Target of TORC1 in Saccharomyces cerevisiae. Mol Cell. 2007; 26: 663–674. https://doi.org/10.1016/j. molcel.2007.04.020 PMID: 17560372

60. Costanzo M, VanderSluis B, Koch EN, Baryshnikova A, Pons C, Tan G, et al. A global genetic interaction network maps a wiring diagram of cellular function. Science (80-). 2016; 353: aaf1420–aaf1420. https://doi.org/10.1126/science.aaf1420 PMID: 27708008

61. Wei Y, Zheng XFS. Nutritional Control of Cell Growth via TOR Signaling in Budding Yeast. In: Castrillo JI, Oliver SG, editors. Yeast Systems Biology. Totowa, NJ: Humana Press; 2011. pp. 307–319. https://doi.org/10.1007/978-1-61779-173-4_18

62. Chen H, Fan M, Pfeffer LM, Laribee RN. The histone H3 lysine 56 acetylation pathway is regulated by target of rapamycin (TOR) signaling and functions directly in ribosomal RNA biogenesis. Nucleic Acids Res. 2012; 40: 6534–6546. https://doi.org/10.1093/nar/gks345 PMID: 22553361

63. Huber A, French SL, Tekotte H, Yerlikaya S, Stahl M, Perepelkina MP, et al. Sch9 regulates ribosome biogenesis via Stb3, Dot6 and Tod6 and the histone deacetylase complex RPD3L. EMBO J. Nature Publishing Group; 2011; 30: 3052–3064. https://doi.org/10.1038/emboj.2011.221 PMID: 21730963

64. Laplante M, Sabatini DM. mTOR signaling at a glance. J Cell Sci. 2009; 122: 3589–3594. https://doi. org/10.1242/jcs.051011 PMID: 19812304

65. Schuldiner M, Collins SR, Weissman JS, Krogan NJ. Quantitative genetic analysis in Saccharomyces cerevisiae using epistatic miniarray profiles (E-MAPs) and its application to chromatin functions. Methods. 2006; 40: 344–52. https://doi.org/10.1016/j.ymeth.2006.07.034 PMID: 17101447

66. Solomon SR. A comparison of ranking methods for normalizing scores [Internet]. Wayne State University. 2008. Available: https://search.proquest.com/docview/304444664

67. Kravatsky Y V., Chechetkin VR, Tchurikov NA, Kravatskaya GI. Genome-wide study of correlations between genomic features and their relationship with the regulation of gene expression. DNA Res. 2015; 22: 109–119. https://doi.org/10.1093/dnares/dsu044 PMID: 25627242

68. Ramírez F, Ryan DP, Grüning B, Bhardwaj V, Kilpert F, Richter AS, et al. deepTools2: a next generation web server for deep-sequencing data analysis. Nucleic Acids Res. 2016; 44: W160–W165. https://doi.org/10.1093/nar/gkw257 PMID: 27079975

69. Weiner A, Hsieh THS, Appleboim A, Chen H V., Rahat A, Amit I, et al. High-resolution chromatin dynamics during a yeast stress response. Mol Cell. The Authors; 2015; 58: 371–386. https://doi.org/ 10.1016/j.molcel.2015.02.002 PMID: 25801168

70. Bonnet J, Wang C-Y, Baptista T, Vincent SD, Hsiao W-C, Stierle M, et al. The SAGA coactivator complex acts on the whole transcribed genome and is required for RNA polymerase II transcription. Genes Dev. 2014; 28: 1999–2012. https://doi.org/10.1101/gad.250225.114 PMID: 25228644

71. Thornton JL, Westfield GH, Takahashi Y -h., Cook M, Gao X, Woodfin AR, et al. Context dependency of Set1/COMPASS-mediated histone H3 Lys4 trimethylation. Genes Dev. 2014; 28: 115–120. https:// doi.org/10.1101/gad.232215.113 PMID: 24402317

72. Lee J-S, Garrett AS, Yen K, Takahashi Y-H, Hu D, Jackson J, et al. Codependency of H2B monoubiquitination and nucleosome reassembly on Chd1. Genes Dev. 2012; 26: 914–919. https://doi.org/10. 1101/gad.186841.112 PMID: 22549955

73. Dutta A, Gogol M, Kim J-H, Smolle M, Venkatesh S, Gilmore J, et al. Swi/Snf dynamics on stress-responsive genes is governed by competitive bromodomain interactions. Genes Dev. 2014; 28: 2314–2330. https://doi.org/10.1101/gad.243584.114 PMID: 25319830

74. McKnight JN, Boerma JW, Breeden LL, Tsukiyama T. Global Promoter Targeting of a Conserved Lysine Deacetylase for Transcriptional Shutoff during Quiescence Entry. Mol Cell. Elsevier Inc.; 2015; 59: 732–743. https://doi.org/10.1016/j.molcel.2015.07.014 PMID: 26300265

75. Gu M, Naiyachit Y, Wood TJ, Millar CB. H2A.Z marks antisense promoters and has positive effects on antisense transcript levels in budding yeast. BMC Genomics. 2015; 16: 99. https://doi.org/10.1186/s12864-015-1247-4 PMID: 25765960

76. Jiang C, Pugh BF. A compiled and systematic reference map of nucleosome positions across the Saccharomyces cerevisiae genome. Genome Biol. 2009; 10: R109. https://doi.org/10.1186/gb-2009-10-10-r109 PMID: 19814794

77. Scherens B, Feller A, Vierendeels F, Messenguy F, Dubois E. Identification of direct and indirect targets of the Gln3 and Gat1 activators by transcriptional profiling in response to nitrogen availability in the short and long term. FEMS Yeast Res. 2006; 6: 777–791. https://doi.org/10.1111/j.1567-1364.2006.00060.x PMID: 16879428

78. Gasch a P, Spellman PT, Kao CM, Carmel-Harel O, Eisen MB, Storz G, et al. Genomic Expression Programs in the Response of Yeast Cells to Environmental Changes. Mol Biol Cell. 2000; 11: 4241–4257. https://doi.org/10.1091/mbc.11.12.4241 PMID: 11102521

79. Jorgensen P. A dynamic transcriptional network communicates growth potential to ribosome synthesis and critical cell size. Genes Dev. 2004; 18: 2491–2505. https://doi.org/10.1101/gad.1228804 PMID: 15466158

80. Getz G, Gabriel SB, Cibulskis K, Lander E, Sivachenko A, Sougnez C, et al. Integrated genomic characterization of endometrial carcinoma. Nature. 2013; 497: 67–73. https://doi.org/10.1038/nature12113 PMID: 23636398

81. Weinstein JN, Akbani R, Broom BM, Wang W, Verhaak RGW, McConkey D, et al. Comprehensive molecular characterization of urothelial bladder carcinoma. Nature. Nature Publishing Group; 2014; 507: 315–322. https://doi.org/10.1038/nature12965 PMID: 24476821

82. Pereira B, Chin S-F, Rueda OM, Vollan H-KM, Provenzano E, Bardwell HA, et al. The somatic mutation profiles of 2,433 breast cancers refines their genomic and transcriptomic landscapes. Nat Commun. 2016; 7: 11479. https://doi.org/10.1038/ncomms11479 PMID: 27161491

83. Ciriello G, Gatza ML, Beck AH, Wilkerson MD, Rhie SK, Pastore A, et al. Comprehensive Molecular Portraits of Invasive Lobular Breast Cancer. Cell. 2015; 163: 506–519. https://doi.org/10.1016/j.cell.2015.09.033 PMID: 26451490

84. Koboldt DC, Fulton RS, McLellan MD, Schmidt H, Kalicki-Veizer J, McMichael JF, et al. Comprehensive molecular portraits of human breast tumours. Nature. 2012; 490: 61–70. https://doi.org/10.1038/nature11412 PMID: 23000897

85. Barretina J, Caponigro G, Stransky N, Venkatesan K, Margolin AA, Kim S, et al. The Cancer Cell Line Encyclopedia enables predictive modelling of anticancer drug sensitivity. Nature. Nature Publishing Group, a division of Macmillan Publishers Limited. All Rights Reserved.; 2012; 483: 307–603. Available: http://dx.doi.org/10.1038/nature11003

86. Giannakis M, Mu XJ, Shukla SA, Qian ZR, Cohen O, Nishihara R, et al. Genomic Correlates of Immune-Cell Infiltrates in Colorectal Carcinoma. Cell Rep. The Authors; 2016; 15: 857–865. https://doi.org/10.1016/j.celrep.2016.03.075 PMID: 27149842

87. Seshagiri S, Stawiski EW, Durinck S, Modrusan Z, Storm EE, Conboy CB, et al. Recurrent R-spondin fusions in colon cancer. Nature. Nature Publishing Group; 2012; 488: 660–664. https://doi.org/10.1038/nature11282 PMID: 22895193

88. Muzny DM, Bainbridge MN, Chang K, Dinh HH, Drummond JA, Fowler G, et al. Comprehensive molecular characterization of human colon and rectal cancer. Nature. Nature Publishing Group; 2012; 487: 330–337. https://doi.org/10.1038/nature11252 PMID: 22810696

89. Ceccarelli M, Barthel FP, Malta TM, Sabedot TS, Salama SR, Murray BA, et al. Molecular Profiling Reveals Biologically Discrete Subsets and Pathways of Progression in Diffuse Glioma. Cell. 2016; 164: 550–563. https://doi.org/10.1016/j.cell.2015.12.028 PMID: 26824661

90. Lefebvre C, Bachelot T, Filleron T, Pedrero M, Campone M, Soria JC, et al. Mutational Profile of Metastatic Breast Cancers: A Retrospective Analysis. PLoS Med. 2016; 13: 1–18. https://doi.org/10.1371/journal.pmed.1002201 PMID: 28027327

91. Beltran H, Prandi D, Mosquera JM, Benelli M, Puca L, Cyrta J, et al. Divergent clonal evolution of castration-resistant neuroendocrine prostate cancer. Nat Med. Nature Publishing Group, a division of Macmillan Publishers Limited. All Rights Reserved.; 2016; 22: 298–305. Available: https://doi.org/10.1038/nm.4045 PMID: 26855148

92. Cancer Genome Atlas Research Network. Integrated genomic analyses of ovarian carcinoma. Nature. 2011; 474: 609–15. https://doi.org/10.1038/nature10166 PMID: 21720365

93. Campbell JD, Alexandrov A, Kim J, Wala J, Berger AH, Pedamallu CS, et al. Distinct patterns of somatic genome alterations in lung adenocarcinomas and squamous cell carcinomas. Nat Genet. Nature Publishing Group, a division of Macmillan Publishers Limited. All Rights Reserved.; 2016; 48: 607–616. Available: https://doi.org/10.1038/ng.3564 PMID: 27158780

94.   Witkiewicz AK, McMillan EA, Balaji U, Baek G, Lin W-C, Mansour J, et al. Whole-exome sequencing of pancreatic cancer defines genetic diversity and therapeutic targets. Nat Commun. Nature Publishing Group; 2015; 6: 6744. https://doi.org/10.1038/ncomms7744 PMID: 25855536

95.   Kumar A, Coleman I, Morrissey C, Zhang X, True LD, Gulati R, et al. Substantial interindividual and limited intraindividual genomic diversity among tumors from men with metastatic prostate cancer. Nat Med. Nature Publishing Group, a division of Macmillan Publishers Limited. All Rights Reserved.; 2016; 22: 369–378. Available: https://doi.org/10.1038/nm.4053 PMID: 26928463

96.   Abeshouse A, Ahn J, Akbani R, Ally A, Amin S, Andry CD, et al. The Molecular Taxonomy of Primary Prostate Cancer. Cell. 2015; 163: 1011–1025. https://doi.org/10.1016/j.cell.2015.10.025 PMID: 26544944

97.   Barretina J, Taylor BS, Banerji S, Ramos AH, Lagos-Quintana M, DeCarolis PL, et al. Subtype-specific genomic alterations define new targets for soft-tissue sarcoma therapy. Nat Genet. Nature Publishing Group, a division of Macmillan Publishers Limited. All Rights Reserved.; 2010; 42: 715–721. Available: https://doi.org/10.1038/ng.619 PMID: 20601955

98.   Bass AJ, Thorsson V, Shmulevich I, Reynolds SM, Miller M, Bernard B, et al. Comprehensive molecular characterization of gastric adenocarcinoma. Nature. Nature Publishing Group; 2014; 513: 202–209. https://doi.org/10.1038/nature13480 PMID: 25079317

99.   Kim J, Bowlby R, Mungall AJ, Robertson AG, Odze RD, Cherniack AD, et al. Integrated genomic characterization of oesophageal carcinoma. Nature. 2017; 541: 169–175. https://doi.org/10.1038/nature20805 PMID: 28052061

100.   Cerami E, Gao J, Dogrusoz U, Gross BE, Sumer SO, Aksoy BA, et al. The cBio Cancer Genomics Portal: An Open Platform for Exploring Multidimensional Cancer Genomics Data: Figure 1. Cancer Discov. 2012; 2: 401–404. https://doi.org/10.1158/2159-8290.CD-12-0095 PMID: 22588877

101.   Ciriello G, Cerami E, Sander C, Schultz N. Mutual exclusivity analysis identifies oncogenic network modules. Genome Res. 2012; 22: 398–406. https://doi.org/10.1101/gr.125567.111 PMID: 21908773

102.   Gao J, Aksoy BA, Dogrusoz U, Dresdner G, Gross B, Sumer SO, et al. Integrative Analysis of Complex Cancer Genomics and Clinical Profiles Using the cBioPortal. Sci Signal. 2013; 6: pl1–pl1. https://doi.org/10.1126/scisignal.2004088 PMID: 23550210

103.   Ebbert R, Birkmann a, Schüller HJ. The product of the SNF2/SWI2 paralogue INO80 of Saccharomyces cerevisiae required for efficient expression of various yeast structural genes is part of a high-molecular-weight protein complex. Mol Microbiol. 1999; 32: 741–51. Available: http://www.ncbi.nlm.nih.gov/pubmed/10361278 PMID: 10361278

104.   Reinke A, Chen JC-Y, Aronova S, Powers T. Caffeine Targets TOR Complex I and Provides Evidence for a Regulatory Link between the FRB and Kinase Domains of Tor1p. J Biol Chem. 2006; 281: 31616–31626. https://doi.org/10.1074/jbc.M603107200 PMID: 16923813